NANO · MICRO small
www.small-journal.com

Electronic Devices Based on Heterostructures of 2D Materials and Self-Assembled Monolayers

Mengmeng Li, Yu Jiang, Hongyu Ju, Suhang He, Chuancheng Jia,* and Xuefeng Guo**

2D materials (2DMs), known for their atomically ultrathin structure, exhibit remarkable electrical and optical properties. Similarly, molecular self-assembled monolayers (SAMs) with comparable atomic thickness show an abundance of designable structures and properties. The strategy of constructing electronic devices through unique heterostructures formed by van der Waals assembly between 2DMs and molecular SAMs not only enables device miniaturization, but also allows for convenient adjustment of their structures and functions. In this review, the fundamental structures and fabrication methods of three different types of electronic devices dominated by 2DM-SAM heterojunctions with varying architectures are timely elaborated. Based on these heterojunctions, their fundamental functionalities and characteristics, as well as the regulation of their performance by external stimuli, are further discussed.

1. Introduction

As the channel length of metal-oxide-semiconductor field-effect transistors (MOSFETs) shrinks to the nanoscale, the short-channel effect of MOSFETs becomes more and more obvious, limiting further miniaturization of devices. From traditional planar transistors to 3D fin field-effect transistors (FinFETs) and to next-generation gate-all-around (GAA) FETs, the current control capability of the gate has been further improved. However, if the focus is turned to the construction materials of devices in combination with their structural designs, the goals of functional tunability and device miniaturization can be achieved by selecting nanoscale materials that are regulated by external stimuli.

2DMs, including graphene (Gr), transition metal dichalcogenides (TMDs), black phosphorus (BP), emerging layered materials, etc., are layered materials with atomic thickness. Different 2DMs have distinct properties such as carrier mobility, bandgap width, optical absorption, etc. Similarly, due to the diversity of molecules, single-molecule thick self-assembled monolayers (SAMs) have various properties such as photoisomerization,[1] redox,[2] dipole,[3] chirality,[4] and other properties. By using these heterostructure of 2DMs and molecular SAMs, the interfacial properties of devices can be modulated, such as reducing the Schottky barrier generated by the contact between 2DMs and metals.[5] In addition, the combination of molecular and 2DM characteristics can realize specific functions, such as molecular optical switch,[6] molecular rectifier,[7] 2DM sensor,[8] etc. Therefore, devices based on 2DM-SAM heterojunctions can greatly enhance the functional richness and tunability of the devices while meeting the requirements of miniaturization.

In this review, we introduce three types of electronic devices composed of 2DM-SAM heterojunctions, primarily covering their structures, mechanisms, and functions. By classifying the direction of current transmission and the relationship between the positions of the two electrodes, two main categories of devices are presented: vertical tunneling devices and horizontal conducting devices. In addition, a category of 2DM-SAM heterojunction devices with intercalation structures are discussed, although such devices can be categorized into vertical and horizontal structures. Finally, an outlook on the prospects of 2DM-SAM heterojunction devices are provided. We hope that this review will provide useful insights and inspiration for researchers and contribute to the ongoing advancement of this field.

2. Vertical Tunneling 2DM-SAM Heterojunctions

In most vertical devices, molecular SAMs are assembled between two electrodes, forming a basic "electrode-SAM-electrode" heterostructure. 2DMs, especially graphene, benefiting from their atomic thickness and high carrier mobility, are excellent electrode materials of SAMs with minimal heterojunction size. The contact

M. Li, Y. Jiang, H. Ju, S. He, C. Jia, X. Guo
Center of Single-Molecule Sciences
Institute of Modern Optics
Frontiers Science Center for New Organic Matter
Tianjin Key Laboratory of Micro-scale Optical Information Science and Technology
College of Electronic Information and Optical Engineering
Nankai University
38 Tongyan Road, Jinnan District, Tianjin 300350, P. R. China
E-mail: she@nankai.edu.cn; jiacc@nankai.edu.cn; guoxf@pku.edu.cn
H. Ju
School of Pharmaceutical Science and Technology
Tianjin University
92 Weijin Road, Nankai District, Tianjin 300072, P. R. China
X. Guo
Beijing National Laboratory for Molecular Sciences
National Biomedical Imaging Center
College of Chemistry and Molecular Engineering
Peking University
Beijing 100871, P. R. China

The ORCID identification number(s) for the author(s) of this article can be found under https://doi.org/10.1002/smll.202402857

DOI: 10.1002/smll.202402857

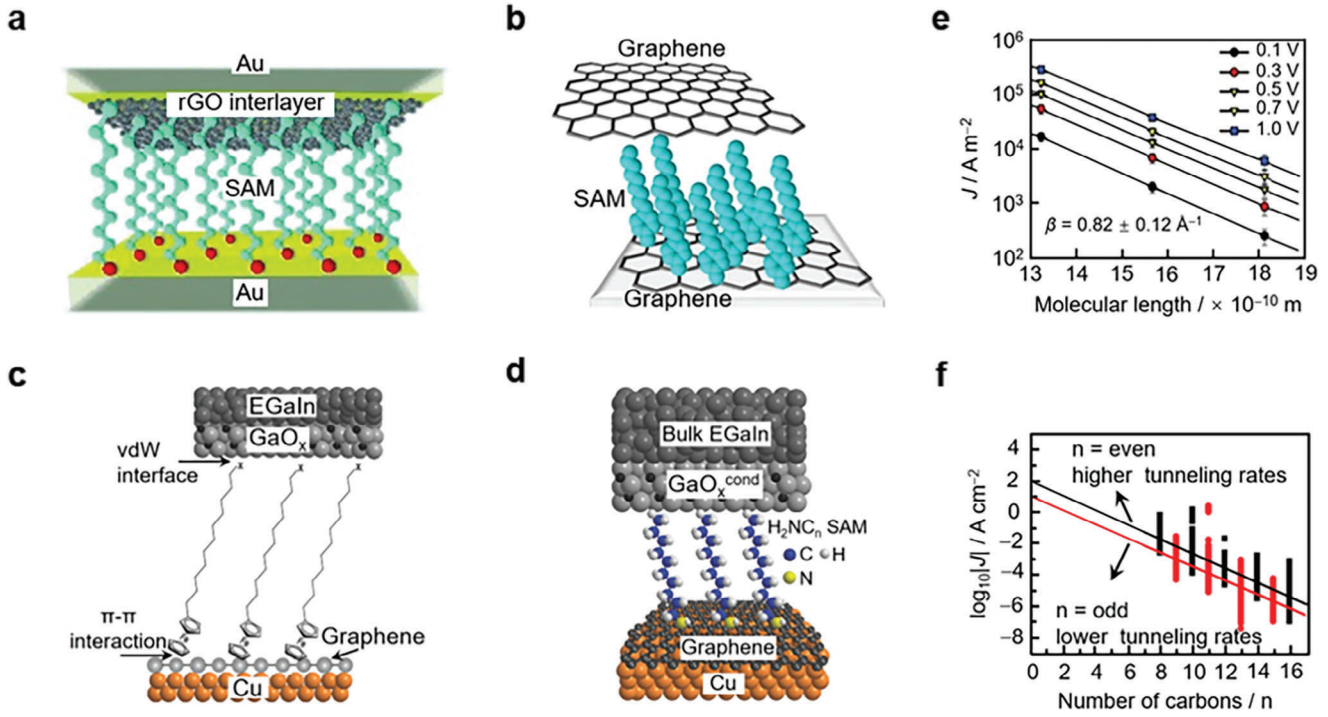

Figure 1. Vertical tunneling devices based on "2DM-SAM" heterojunctions. a,b) Vertical tunneling devices formed by covalent bonding on the metal electrode (a) and the Gr electrode (b). a) Reproduced with permission.[11a] Copyright 2012, Wiley-VCH. b) Reproduced with permission.[6] Copyright 2013, Springer Nature. c,d) Vertical tunneling devices formed by π– π interaction with the Gr electrode (c) and non-covalent interactions between amino groups and the Gr electrode (d). c) Reproduced with permission.[9a] Copyright 2018, Wiley-VCH. d) Reproduced with permission.[9b] Copyright 2015, Wiley-VCH. e) Relationship between the molecular length of alkanethiol and the current density of vertical tunneling devices. Reproduced with permission.[11a] Copyright 2012, Wiley-VCH. f) Odd-even effect in vertical tunneling devices. Reproduced with permission.[17] Copyright 2017, American Chemical Society.

between 2DMs and SAMs can be established through soft van der Waals (vdW) interactions or covalent bonds. Inserting 2DM between SAM and metal electrodes prevents irreversible damage to the SAM that can result from direct deposition of metal electrodes. Based on this structure, extensive research has been conducted on the fundamental electrical properties of SAMs and the interactions between SAMs and electrodes.[6,9] In addition, the properties of SAMs modulated by external stimuli (such as light, electric field, temperature, electrochemical means, etc.) were also investigated.[6,10]

2.1. Construction of Molecular SAMs

The vertical 2DM-SAM devices, designed to explore the fundamental properties of SAMs, were fabricated using different approaches and exhibit diverse structures. These devices can be classified based on the electrode materials used for assembling molecular SAMs into those with SAMs on metal electrodes and those with SAMs on 2D materials. Electron transport in heterojunctions can be either coherent or incoherent, depending on whether the electrons interact with the molecules. Coherent transport is primarily governed by the tunneling mechanism. During incoherent transport, where the molecular size is generally larger, electrons are scattered by molecules, and the transport is dominated by the hopping mechanism. Besides the type of molecule and electrode, the electron transport mechanism is also influenced by external factors such as bias and temperature.

For vertical devices with molecular SAMs on metal electrodes, the molecules are preassembled by covalent bonds to form a monolayer on the metal bottom electrodes, followed by placing the top electrodes. This approach requires anchoring groups, such as– SH or– NH_2 at the end of molecules, to form covalent bonds like Au– S with the metal electrode, ensuring the creation of a firmly assembled monolayer. While, in theory, a molecular device can be formed through the contact of molecules with the metal electrodes on both upper and lower sides, practical preparation processes often yield SAMs that are only a few nanometers thick. Therefore, there is a strong preference for establishing a soft contact between the SAM and the metal electrode.

A vertical molecular device, following the structure of "metal-2DM-SAM-metal," can be fabricated by spin-coating well-dispersed reduced graphene oxide (rGO) sheets in a solution onto a bottom Au electrode, with the molecular monolayer preassembled covalently. Subsequently, a top Au electrode layer is slowly evaporated onto the rGO (**Figure 1a**). In comparison with monolayer Gr, rGO is a more cost-effective choice, as it can be conveniently produced through spin-coating, without the need for chemical vapor deposition and transfer steps. The rGO interlayer serves to decrease the likelihood of the molecular damage or short circuits resulting from metal atoms penetrating the SAM during the direct metal deposition process, thus realizing the

authentic molecular effects in molecular devices.[11] In addition, the devices exhibited minimal degradation even after 30 days in a vacuum, demonstrating the dependable capability of 2DM rGO to provide stable molecular transport properties. Figure 1b shows the assembly of aryl diazonium molecules onto the sp^2 hybridized Gr through a dediazoniation process, a chemical reaction employed for functionalizing Gr surfaces.[6,12] This covalent connection, characterized by strong coupling, enhances the stability of the 2DM-SAM heterojunction. Consequently, the formation of a covalently linked 2DM-SAM heterojunction implies the occurrence of a corresponding chemical reaction between the electrode surface and the molecular attachment points.

From a molecular energy level perspective, excessively strong coupling between molecules and electrodes results in a significant broadening of molecular orbitals,[9a] which is unfavorable for the rectification effect of the device.[13] The rectification effect involving molecules containing ferrocene (Fc) units was reported by using the π-π interaction between molecules and Gr to form a monolayer of Fc-terminated molecules on the surface of Gr electrodes (Figure 1c). The π-π interaction, being a weak non-covalent force, prevents the broadening of molecular orbitals, ensuring the smooth assembly of molecules on Gr.

An alternative non-covalent method for assembling molecules is to use the vdW interaction between the- NH_2 group at the end of the molecule and the Gr to form a SAM (Figure 1d). This interaction maintains the sp^2 hybridization of Gr, resulting in an effective tunneling barrier for the junction (i.e., a tunneling decay coefficient of 1.02 ± 0.08 $n_C{}^{-1}$, where n_C is the number of C atoms). Moreover, compared to molecular monolayers assembled via organothiolate-metal bonds, those assembled in this manner are not easily decomposed under ambient conditions. The Cu//Gr//H_2NC_n//$GaO_x{}^{cond}$/EGaIn tunneling junctions constructed in this way maintain their electrical properties in ambient conditions for more than 30 days.[9b,14]

The alkanethiol monolayer assembled between the two electrodes behaves as a passive molecular resistance. The conductivity of the alkanethiol device correlates directly with the thickness of the SAM, with more C atoms indicating a longer tunneling distance and lower conductivity. Figure 1e shows the current densities of three alkanethiol devices with varying lengths at different bias voltages. The average tunneling attenuation factor β is measured to be 0.82 ± 0.12 $Å^{-1}$, which is consistent with previously reported values for alkanethiol junctions.[11a,15]

The vertical tunneling junction is also an excellent structure for the study of interfacial effects between SAMs and materials. An odd-even effect in the tunneling rate is observed in junctions based on SAMs with an alkyl skeleton, where CH_2 is the repeating unit. In previous studies, strong covalent interaction was used to assemble the molecular monolayer with fixed bond angles between the SAM and bottom electrode, resulting in an odd-even effect of the molecular end groups.[16] Furthermore, the odd-even effect of the tunneling rate is also observed in junctions with the molecular monolayer assembled by vdW interaction between the molecular end group- NH_2 and the bottom Gr electrode (Figure 1f). This suggests that the odd-even effect is independent of rigid bond angles between the SAM and bottom electrode.[17] This result inspires further exploration of molecule properties and molecule-electrode interactions using vertical tunneling SAM devices.

2.2. Regulation of Devices Properties

2DMs, typically represented by Gr and TMDs, play an important role in optical, electric field and electrochemical regulation of vertical SAM tunneling devices. For example, as the top electrode in the device, Gr is characterized by its ability to allow the transmission of light, electrostatic fields, and electrons, which greatly facilitates the direct manipulation of SAM properties through external stimuli. Moreover, the regulated SAM, in turn, influences the properties of the 2DMs.

2.2.1. Devices Based on Gr-SAM Heterostructures

There are many ways to manipulate the properties of vertical 2DM-SAM heterojunction devices, most of current researches are focused on the inherent characteristics of the SAMs.[18] In the case of light regulated vertical 2DM-SAM heterojunction devices, specific conditions must be met for effective regulation. First, the molecules assembled on the bottom electrode should be photosensitive to ensure responsiveness to light stimulation. Second, the material selection or structural design of the heterojunction device should enable efficient irradiation of the SAM by light, a prerequisite for regulating device properties through light. In comparison to previous vertical devices using metal electrodes, a single layer of 2DMs, whether Gr or TMDs, as electrodes offer good light transmittance. Thus, the structure of vertical 2DM-SAM heterojunctions meets the latter condition mentioned above.

In response to the above requirements, many photoisomerized molecules with photosensitive properties have been used to prepare functional vertical SAM devices,[1,6,10c,19] including azobenzene (Azo), a common photoisomerization unit that can be converted into a *cis* or *trans* structure when exposed to ultraviolet or visible light. The Gr-SAM-Gr vertical device constructed from aryl azobenzene molecules covalently assembled on Gr allows irradiation to regulate Azo units in SAM (**Figure 2**a). Figure 2b shows the current density plots for reversible optical switching cycles, where the ultraviolet-irradiated *cis*-isomer SAM exhibits a higher conductivity state than the *trans*-isomer, attributed to the shorter tunneling distance of the *cis*-isomer SAM.[6]

Diarylethene (DAE), another widely studied photoisomerization unit, is capable of transitioning between the open-ring and closed-ring structures upon exposure to ultraviolet or visible light. Figure 2c shows the structures of two vertical SAM devices featuring DAE as the functional unit, with Au serving as the bottom electrode and multilayer rGO as the top electrode. The switching ratio of the device resulting from photoisomerization of the SAM can reach up to two orders of magnitude (Figure 2d). However, due to the strong coupling between the closed state molecules and the electrodes, the switching function of the device is unidirectional, meaning that it can only switch from a low conductivity state to a high conductivity state, and vice versa.[19] This strong coupling can be mitigated by designing a proper molecular length.[20]

Another photoisomerization system worth mentioning is the dihydroazulene (DHA)/vinylheptafulvene (VHF) system, although has received less attention previously. As shown in Figure 2e, the molecules are assembled onto the Au electrode,

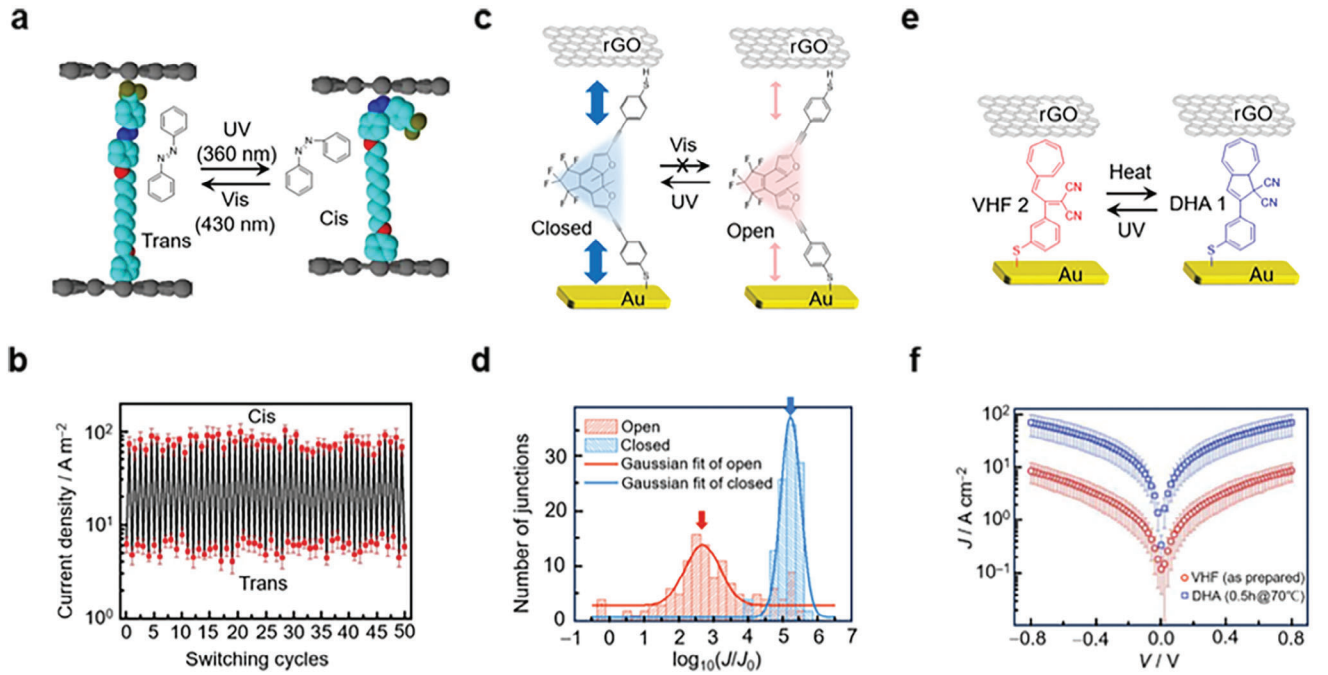

Figure 2. Photo-regulated vertical tunneling switching device based on "Gr-SAM" heterojunction. a,c,e) Schematic diagram of the optical switching device with the Azo unit (a), the DAE unit (c), and the DHA1/VHF2 unit (e). b,d,f) The electrical performance of the optical switching device with the Azo unit (b), the DAE unit (d), and the DHA1/VHF2 unit (f). a,b) Reproduced with permission.[6] Copyright 2013, Springer Nature. c,d) Reproduced with permission.[19] Copyright 2019, American Chemical Society. e,f) Reproduced with permission.[10c] Copyright 2013, Wiley-VCH.

with rGO as the top electrode. A DHA derivative, namely DHA1, can transform into the corresponding VHF derivative VHF2 by ring-opening reaction upon ultraviolet irradiation. The latter can then convert back to DHA1 through thermal activation. Therefore, the bidirectional switching characteristic of the SAM device can thus be induced by heating and ultraviolet irradiation, however, the switching ratio is not very high (<10) (Figure 2f).[10c]

It is noteworthy that the optical switching behavior of photoisomerized molecular devices is inherently slow, which is constrained by the rate of conformational transformation. For example, in the case of the SAM device with DAE (Figure 2c), the state-switching process requires 613 s.[19] Similarly, the optical switching process for the SAM device featuring Azo as the functional unit, as shown in Figure 2a, also exhibits a slow transition.[6]

In addition, an external electric field can also serve as an effective physical means to modulate the tunneling characteristics of vertical tunneling vdW heterojunctions by adjusting specific energy levels, in the premise of the partial electrostatic transparency of Gr. **Figure** 3a shows a vertical tunneling heterojunction structure that uses an electric field generated by an electric double layer (EDL) of an ionic liquid gate to regulate the tunneling current between the Gr electrode and the metal electrode. In detail, the gate electric field penetrates the Gr layer, finely tuning the energy level of the SAM relative to the Dirac point of Gr (Figure 3b), and consequently impacting the electron tunneling rate, thereby achieving the regulation of the conductance by the gate electric field. Therefore, SAM devices based on this regulatory mechanism are expected to achieve higher switching ratios through reasonable selections of energy levels of molecules and electrodes. For example, Figure 3c shows the J_{ds}–V_{ds} characteristic curves of a SAM experiencing destructive quantum interference effects under the control of a gate electric field, exhibiting a higher switching ratio compared to a SAM in the absence of electric field modulation.[10a,b,21]

To enable the chemical regulation of 2DM-SAM heterojunction properties, it is essential, on one hand, for the molecule to respond to the chemical environment and thereby alter certain characteristics of the molecule. On the other hand, changes in certain characteristics of the molecule should be translated into alterations in some properties of the device. As shown in Figure 3d, a vertical device is proposed based on a Gr-SAM-Au heterojunction, where Fc serves as a functional unit in the molecule with redox properties. Electrons can transfer through Gr between an oxidizing reagent (such as H_2O_2 solution) or reducing reagent (such as $NaBH_4$ solution) outside the device and a SAM inside the device, capitalizing on Gr electron permeability and the impermeability of most ions. In detail, as shown in Figure 3e, the Fc unit can lose an electron to undergo a chemical reduction reaction (C-reduction) (left). Conversely, the positively charged Fc unit can obtain an external electron, undergoing a chemical oxidation reaction (C-oxidation) (right), while improving the coupling strength of the Gr and Fc functional units, thereby increasing the conductance of the device. For devices treated sequentially by oxidizing (red) and reducing (green) solutions, $|J_{ds}|$ at $V_{ds} = -0.5$ V is shown in Figure 3f, which achieves a switching ratio of more than two orders of magnitude.[2]

In addition to switching devices where the SAM is positioned between the source and drain electrodes, there is also a less-explored photovoltaic device configuration where the SAM is situated outside the two electrodes, capitalizing on the

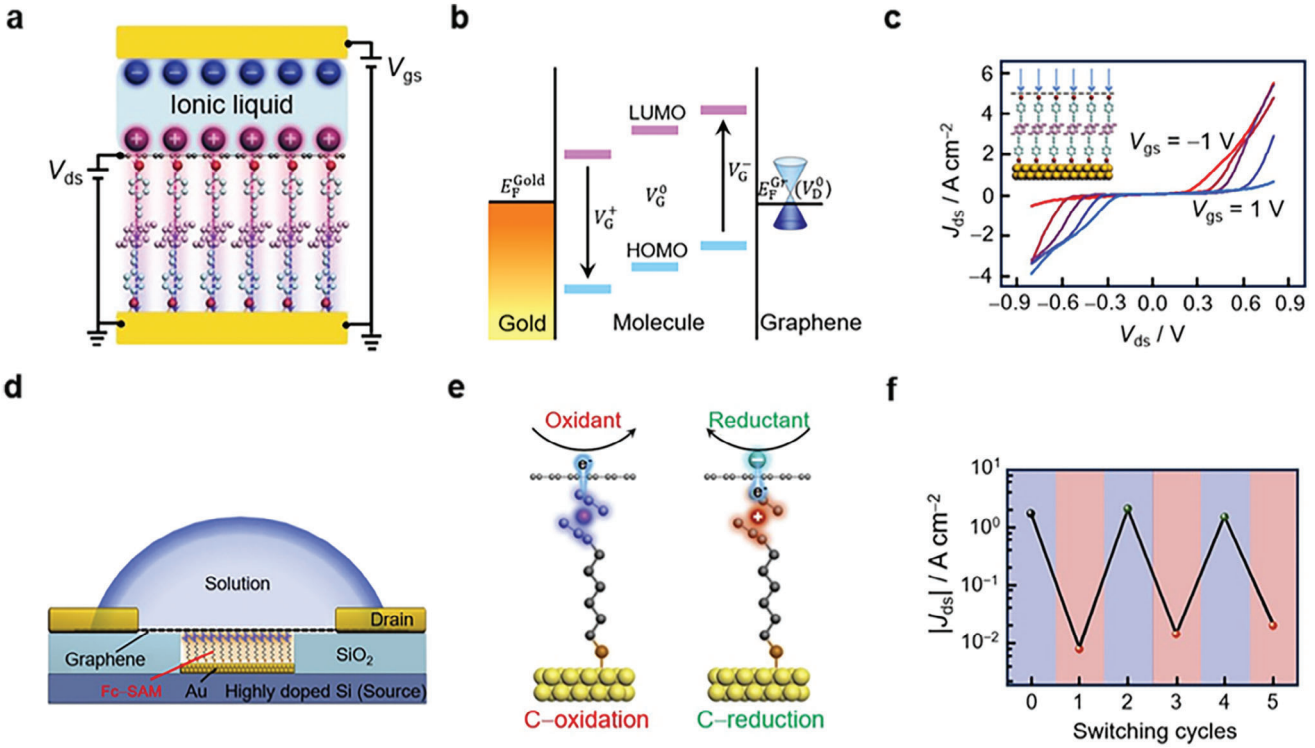

Figure 3. Vertical tunneling switching devices with electric field and chemical regulation. a) Schematic diagram of the electric field-regulated device. b) Energy level structure with gate voltage regulation. c) J_{ds}–V_{ds} curves with gate voltage regulation. Reproduced with permission.[10b] Copyright 2018, American Association for the Advancement of Science. d) Schematic diagram of the chemically regulated device structure. e) SAM redox in vertical device. f) Switching performance of chemically regulated vertical devices. Reproduced with permission.[2] Copyright 2020, Elsevier Inc.

electron permeability of Gr. The SAM of photoactive molecules acts as an organic layer within these vertical photovoltaic devices.[22]

The dye molecule Acridine Orange (AO) has been employed in the fabrication of such photovoltaic devices. **Figure** 4a,b shows, respectively, the structural diagram of a TiO_2/SLG/AO ternary interface device with polymethyl methacrylate protective layer and cross sectional high-resolution dark field scanning transmission electron microscopy (STEM) images. Different from the mechanisms and performances of conventional organic semiconductor photovoltaic devices, this TiO_2/Gr/SAM heterostructure, based on the ipsilateral selective electron tunneling (ISET) mechanism, exhibits an ultrahigh absorbed photon-to-current efficiency. In the ISET mechanism, the photogenerated electron-hole pairs in the SAM on one side of Gr are separated. Electrons tunnel through the electron-permeable Gr to the TiO_2 layer, while the holes are blocked. The following two examples of TiO_2-Gr-SAM ternary interfaces illustrate in detail this important mechanism in photovoltaic devices.

The unique interfacial electronic structure leads to the ipsilateral separation of the photogenerated carriers and selective ballistic electron tunneling across Gr to the TiO_2 layer. Figure 4c shows the projected density of states (PDOS) spectra, showing the electron band structure of the TiO_2/SLG/AO ternary interface. The lowest unoccupied molecular orbit (LUMO) of AO lies at ≈−2.7 eV relative to the vacuum energy level, matching well with the unoccupied electron states of the adjacent Gr, which are strongly coupled to the conduction band (CB) states of TiO_2. Simultaneously, the highest occupied molecular orbit (HOMO) of AO is ≈−5.0 eV, matching the occupied states of Gr, while the valence band (VB) maximum of TiO_2 is ≈−7.3 eV. Therefore, the electron permeability of monolayer Gr enables the photoexcited electrons in the SAM to traverse through Gr and ballistically inject into the CB of TiO_2, whereas the holes cannot, ensuring effective separation of photoexcited electrons and holes. Moreover, the process of electron tunneling into TiO_2 (89 fs) is much faster than the energy relaxation (5.1 ps) and recombination (17.8 ps) processes of the injected electrons, allowing for a high electron collection efficiency (97.8%). Subsequently, the electrons are directed to the external circuit for use by the load, thereby achieving the photovoltaic function of the device (Figure 4d).

Z907 ruthenium, a dye molecule with high photoactivity and unique amphiphilic structure, has been widely used as the dye sensitizer in solar cells.[22a,23] Similar to the AO molecular device mentioned above, the Z907 molecule also realizes a photovoltaic device with good performance based on TiO_2/Gr/SAM heterostructure and ISET mechanism. Figure 4e shows the photoinduced carrier generation, separation, and transport in photovoltaic devices, with the principle consistent with that presented in Figure 4c. For a charge density of −3.7 eV, electrons demonstrate direct tunneling from Z907 to TiO_2 (Figure 4e, upper right), while, for a charge density of −5.2 eV, holes transfer from Z907 to SLG (Figure 4e, lower right). The current-voltage characteristics are shown in Figure 4f, including conditions

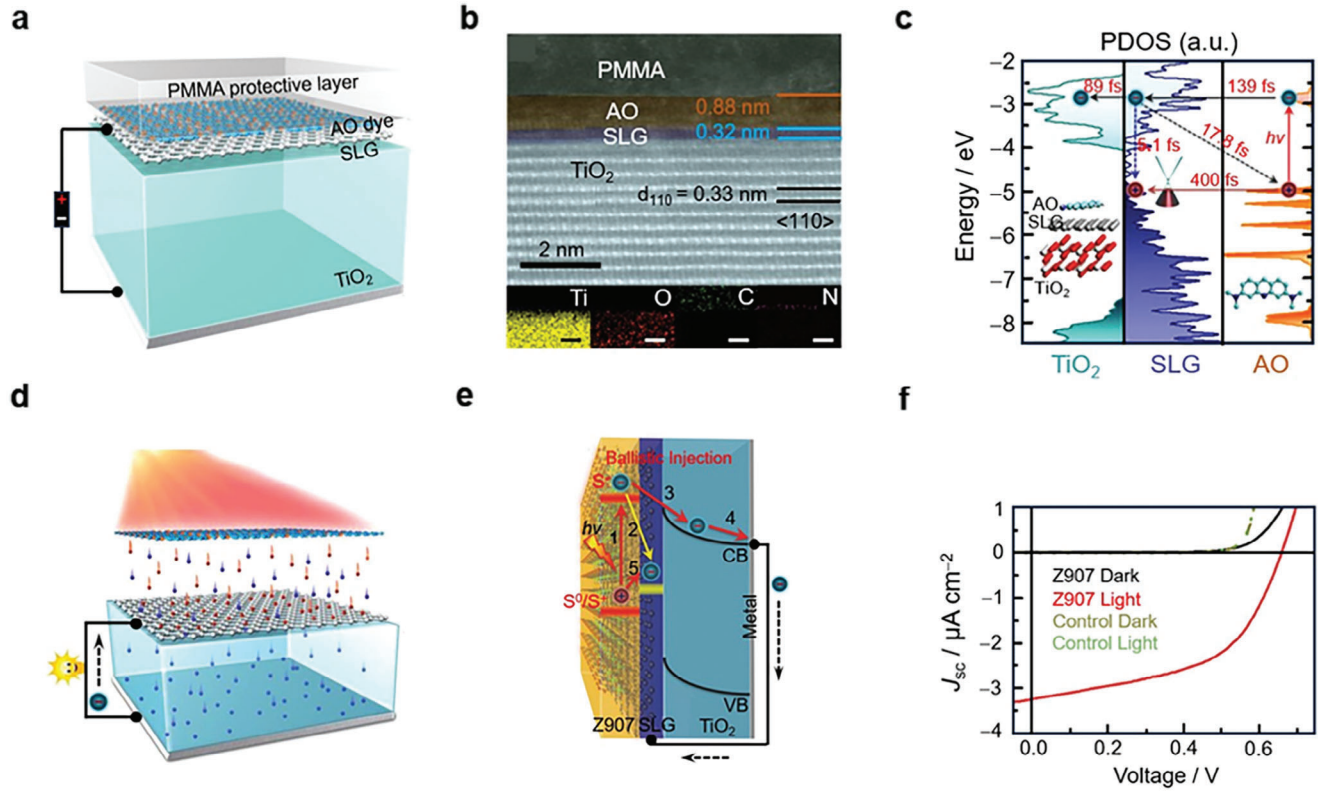

Figure 4. Ipsilateral selective tunneling photovoltaic devices based on "Gr-SAM" heterojunction. a) Structure of the photovoltaic device with a TiO_2/SLG/AO ternary interface. b) Cross sectional high-resolution dark-field STEM image of the TiO_2/SLG/AO ternary interface. c) PDOS spectra for TiO_2, SLG, and AO. d) Schematic diagram of the photovoltaic effect mechanism. Reproduced with permission.[22c] Copyright 2016, American Chemical Society. e) Schematic diagram of photoinduced carrier generation, separation, and transport in the photovoltaic device with a Z907/SLG/TiO_2 ternary interface. f) J_{sc}–V curves of the Z907/SLG/TiO_2 photovoltaic device and a control device without the Z907 dye in both dark and light conditions. Reproduced with permission.[22a] Copyright 2017, Wiley-VCH.

both in darkness and under light, and with or without Z907 molecules. Under illumination, Z907 has an open-circuit voltage (V_{oc}) of ≈0.663 V and a short-circuit current density (J_{sc}) of ≈3.27 μA cm^{-2}, showing its high photovoltaic conversion performance. Crucially, the selection of the SAM and the single layer of Gr in the photovoltaic heterostructure is very important. The higher electron transparency of the single layer of Gr, in comparison to multilayer Gr, coupled with the less photoexcited-hole collection process and reduced electron-hole recombination resulting from the use of a SAM instead of a multilayer of molecules, collectively contribute to a high fill factor (FF) and a high open circuit voltage (V_{oc}) of the photovoltaic device.[22b,24]

2.2.2. Devices Based on TMD-SAM Heterostructures

Monolayer TMDs, characterized as direct bandgap semiconductors, have been widely studied and applied in the field of optoelectronics. In vertical molecular film devices, molecules with different structures can be used to modulate the interface between the SAM and the 2DM electrode, thereby influencing the properties of the 2DM. For example, when monolayer MoS_2 which with obvious photoluminescence (PL) characteristics, is used as the top electrode on the Azo derivative SAM, as shown in **Figure** 5a, light can reversibly regulate the configuration of the Azo unit through the monolayer MoS_2 and further influence the electrical properties of MoS_2 via the doping effect. The qualitative energy level diagram of MoS_2 doped with Azo units is shown in Figure 5b. In the *trans* configuration of the Azo unit, n-type doping occurs on the emission side band of the monolayer MoS_2 electrode. Upon conversion of the molecules from a *trans* to a *cis* configuration, the doping of MoS_2 is reduced, resulting in the quenching of the emission side band and an overall enhancement in PL efficiency (Figure 5c). This achieves photoswitchable optical properties of the monolayer MoS_2.[1]

The devices prepared from the combination of non-functional SAM and photoactive 2DM layer holds the potential for achieving a higher optical switching speed compared to those prepared from photoisomeric molecules. In Figure 5d, a photodiode device comprising a dipolar tridecafluoro-1-octanethiol (F6H2) SAM, a photoactive layer of WSe_2, and Gr has been proposed. The molecular dipole moment induces band alignment of WSe_2 in the WSe_2-SAM interface, enabling the photoswitching capability of the device. An ultrafast photo-response of ≈100 μs has been achieved. The band diagram of the dipole-dependent charge transport mechanism for the WSe_2-SAM heterojunction device is illustrated in Figure 5e. Notably, the band bending of WSe_2 allows the rapid separation of photoexcited electrons and holes by

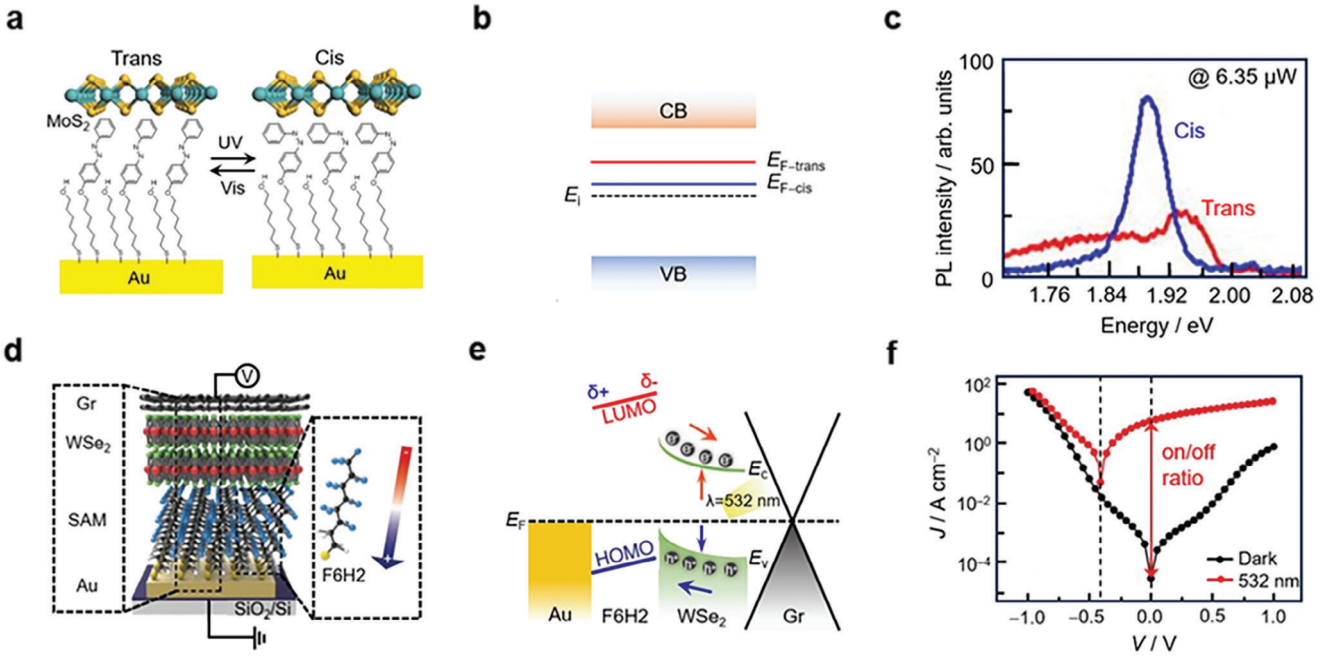

Figure 5. Vertical tunneling devices based on "TMD-SAM" heterojunction. a) Structure of the "MoS_2-Azo SAM" heterojunction-based device. b) Energy levels of MoS_2 doped with two configurations of Azo SAMs. c) PL performance of the "MoS_2-Azo SAM" heterojunction. Reproduced with permission.[1] Copyright 2014, AIP Publishing LLC. d) Structure of the "Gr-WSe_2-dipolar SAM" heterojunction-based device. e) Energy levels of the device with dipolar F6H2 SAM. f) Switching performance of the photoresponsive device. Reproduced with permission.[25] Copyright 2022, Wiley-VCH.

an internal electric field between two electrodes when exposed to light. This implies that a certain photocurrent can be generated rapidly even at zero bias. Conversely, the photocurrent is minimized when the external bias and internal electric field counterbalance each other. In the absence of light, the current is minimized at zero bias, resulting in an optical on/off ratio of up to 1.99×10^5 at zero bias for the device (Figure 5f).[25] The rectification performance of the "Gr-WSe_2-dipole SAM" heterojunction (with a ratio of 10 to100) is not as strong as that of a typical 2D semiconductor heterojunction (usually $> 10^3$). However, it offers unique advantages. By modifying the molecular dipole moment, the rectification and photovoltaic response characteristics of the heterojunction can be conveniently adjusted.

3. Horizontal Conducting 2DM-SAM Heterojunction Devices

In most horizontally conducting 2DM-SAM heterojunction devices, the 2DM is the main electron conduction pathway, while the SAM significantly influences the properties of the 2DM. This is different from the vertical tunneling heterojunctions discussed in the previous chapter, where the SAM functions as the primary electron tunneling pathway, and the 2DM serves as the electrode. Horizontal devices, conducted by the 2DM, can be initially categorized into three types based on the different environments in which 2DM-SAM heterojunctions are connected. In addition, a small number of horizontal conducting 2DM-SAM heterojunction devices rely on the SAM for current conduction.

3.1. Intrinsic 2DM-SAM Heterojunctions

By doping 2DMs, their electrical and optical properties can be conveniently tuned, allowing for the design of devices with specific requirements and a better understanding of their working principles. In comparison with other techniques, such as substitution doping and electric/magnetic field-induced doping, chemical doping using SAMs has the advantage that molecular dopants are versatile and readily available, without the need to consider lattice matching. Additional advantages include the simplicity of the doping procedure, because SAMs can be applied to the 2DM surface through soaking or spinning molecular solutions. However, despite these advantages, the connection between 2DMs and SAMs is generally based on physical adsorption (especially in chemical doping based on charge transfer mechanisms), which is not very stable and easily degrades, resulting in a short device lifetime.

Mechanistically, chemical doping can change the charge transfer between the SAM and the 2DM, which is expected to bring about a shift in the Fermi level of the 2DM, thus regulating its electrical and other properties of 2DMs. The extent of charge transfer signifies the relative electron-donating or -absorbing capacity of the two materials in contact. This characteristic is independent of the molecular connection to the 2DM, whether covalent or non-covalent,[26] and it is also unaffected by the relative positioning of the SAM and the 2DM.[27] **Figure 6a** shows two major horizontal conducting 2DM-SAM heterostructures. The upper configuration is a case where the molecules are assembled on the 2DM. The lower configuration shows a situation where the molecules are assembled on an insulating substrate. Through the introduction of suitable molecular dopants, both

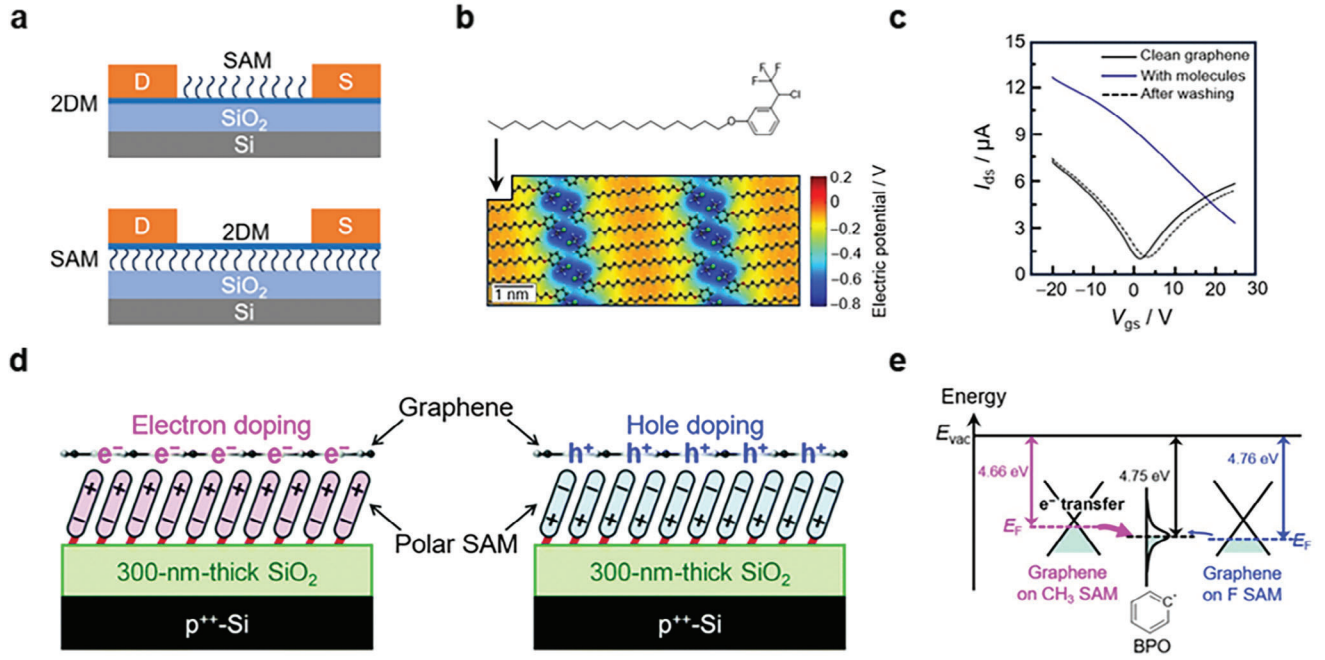

Figure 6. Horizontal conducting devices with "Gr-SAM" heterojunction. a) Schematic presentation of two typical "2DM-SAM" horizontal conduction heterojunction devices with the SAM on the 2DM (upper) or under the 2DM (lower). b) Calculated electrical potential induced by a supramolecular lattice on Gr. c) I_{ds}– V_{gs} transfer characteristic curves of the horizontal device. Reproduced with permission.[31] Copyright 2017, Springer Nature. d) Schematic diagram of electron doping and hole doping effects of SAMs with different dipole orientations on Gr. e) Energy level diagram of the chemical reaction between BPO molecules and the surface of the- CH_3/– F SAM doped-Gr. Reproduced with permission.[39] Copyright 2020, Royal Society of Chemistry.

structures can undergo chemical doping via the charge transfer mechanism. More specifically, if the redox potential of the molecules is situated below the valence band maximum (VBM) of the 2DM, electrons may transfer from the 2DM to the molecules, which possess a strong electron-absorbing ability, resulting in p-type doping.[28] Conversely, when the redox potential of the molecules exceeds the conduction band minimum (CBM) of the 2DM, electrons can transfer from the molecules, which have a strong electron-donating ability, to the 2DM, leading to n-type doping.

Dipolar interaction is another important aspect through which chemical doping regulates the properties of 2DM. When a molecule comes into contact with the 2DM, its dipole moment can apply an electric field to the surface of the 2DM, influencing the intrinsic electronic structure of the latter. Establishing a significant electric field requires the molecules to form a well-organized arrangement. In such conditions, a macroscopic shift of the Fermi level in the 2DM occurs, which allows the carrier density of 2DMs to be controlled. Molecules of varying dipolar orientations and magnitudes can be used to customize the types and sizes of chemical doping.[28a]

To fabricate a horizontal heterojunction device via chemical doping, as showcased by the lower structure in Figure 6a, molecules are intricately designed to covalently assemble on the SiO_2 substrate via their anchoring groups, while also interacting non-covalently with the lower surface of the transferred 2DM. The advantages of this design, first, enables the formation of a SAM with an ordered and compact arrangement of molecules, ensuring the effective regulation of the 2DM by molecular dipoles. Second, employing non-covalent interaction between the SAM and the 2DM can minimize the reduction in carrier density caused by the molecular covalent assembly on its surface.[29] For the heterojunctions based on SiO_2-SAM-Gr structure, the Fermi level shifts of Gr caused by molecules with different dipole moments were studied experimentally and computationally. Monolayers assembled by molecules with larger dipole moments result in more significant Fermi level shifts, while those with opposite dipole moments induce shifts in different directions.[30]

Notably, achieving chemical doping through molecular dipoles can also be realized by the ordered assembly of SAMs on the 2DM surface,[31] in which case it can reduce the susceptibility of 2DMs to ambient conditions. For instance, BP is sensitive to oxygen and humidity due to its threefold coordinated atoms, which compromises performance of BP-based devices in ambient conditions.[32] 2DMs also exhibit enhanced stability in the presence of molecular monolayer. For example, the preservation period of BP-based devices, when coated with the octyltrichlorosilane (OTS) SAM, is extended to over 28 days in ambient air, in sharp contrast to the less than 7 days of stability observed when BP is directly exposed to air.[33] On the other hand, the assembly of certain molecules at surface defect of 2DMs can improve the electron transport and PL properties of these materials. Through the adsorption of organosulfur compounds at sulfur vacancy points on the MoS_2 surface, the sulfhydryl groups play a reparative role in addressing sulfur vacancies within transitional TMDs, thereby effectively inhibiting electron scattering around defect sites.[34]

3.1.1. Devices Based on Gr-SAM Heterostructures

By chemical doping, the electronic structure of Gr that in contact with molecular dopants can be modulated. A Gr surface with high carrier density of over 10^{13} cm^{-2} can be achieved by self-assembling monolayer fluoroalkyl silanes on Gr.[35] By using tetrafluorotetracyanoquinodimethane (F4-TCNQ) molecules with strong electron absorbing capacity to functionalize the Gr surface, the band structure of epitaxial n-type doped Gr on SiC(0001) can be precisely tailored to attain charge neutrality.[36]

For a device with 2DM-SAM heterojunction (Figure 6a, upper), the doping effect on 2DMs can be regulated via molecular conformation changes upon photochemical reactions.[31] By spin-coating a molecular solution onto the Gr surface, the long molecular chains interact with the Gr surface through vdW interactions, whereas the diazirine moiety responds to the light stimulus, forming a supramolecular lattice. Changes in the position of $-CF_3$ relative to the Gr plane after the photochemical reaction result in a modification of the dipole interaction between the SAM and Gr. Consequently, this leads to the realization of 1D periodic potentials of varying magnitudes and controllable doping effects (Figure 6b). The transfer curve of the device after the photochemical reaction, as shown in Figure 6c, indicates that the doping effect of the molecule results in a significantly positive threshold voltage ($V_{gs} > 20$ V) compared to the absence of molecules.

For a device in which the SAM on the substrate is enclosed and separated from the air (Figure 6a, lower), effective chemical doping of 2DMs can be achieved by modifying the terminal groups of the molecule, such as adjusting their electron-donating or electron-absorbing capabilities. As an illustration, 3-aminopropyltriethoxysilane molecules, in their protonated form, are assembled on a SiO_2 substrate through covalent bonds, forming a H_3N^+-SAMs. The positively charged $-NH_3^+$ terminal group contacts the top Gr and absorbs electrons from Gr, resulting in the formation of p-type doped Gr. When a back-gate voltage is applied, a significant threshold voltage ($V_{gs} = 20$ V) is observed on the transfer curve at $V_{ds} = 100$ mV, confirming the presence of p-type doping. In contrast, the self-assembled monolayer of 3-aminopropyltriethoxysilane molecules (H_2N-SAM) contacts the top Gr and donates electrons to Gr through the $-NH_2$ terminal group, which contains lone pair electrons. The corresponding transfer curve shows an opposite threshold voltage ($V_{gs} = -18$ V), indicating that H_2N-SAM supplies electrons to Gr, resulting in n-type doping of Gr.[29b]

In addition, solid-phase reactions on the surface of Gr can be effectively controlled by SAMs. Given the electron-rich nature of Gr, it has a tendency to form chemical bonds with electron-accepting molecules through an electron transfer mechanism, which is intricately correlated to the energy level arrangement of both Gr and molecules.[37] SAMs play an important role in fine-tuning the energy levels of graphene, thereby regulating the ensuing chemical reactions with surface-active molecules. Benzoyl peroxide (BPO), a representative molecule for modifying Gr surfaces, can produce neutral phenyl radicals in the photochemical reaction process, which can selectively absorb electrons from Gr, leading to subsequent reactions and binding with the Gr surface.[37,38] To modulate the photochemical reaction of BPO molecules on Gr, a design involving the use of the electrostatic field generated by a monolayer of dipole molecules has been proposed.[39] As shown in Figure 6d, molecules with specific dipoles, e.g. $-CH_3$ (or $-F$) as terminals, are preassembled on the SiO_2 substrate and selectively introduces electrons (or holes) to the upper Gr. This can effectively adjust the energy levels of Gr, and consequently, control the reaction of BPO molecules on its surface. The study revealed that elevating the energy level of Gr can facilitate the reaction to occur, as the electron transfer from the Gr level to the molecular level is more likely to occur (Figure 6e).

3.1.2. Devices Based on TMD-SAM Heterostructures

As important new 2D semiconductor materials with remarkable electrical and optical properties, TMDs have attracted great interest in recent years. The bandgap of TMDs changes from indirect bandgap to direct bandgap as the thickness decreases from bulk to monolayer.[40] Chemical doping provides an efficient way to convert 2DM into p-type and n-type semiconductors, similar to that in conventional silicon-based semiconductors.

Benzyl viologen (BV) is among the electron-donor organic compounds that has the highest reduction potentials. As shown in **Figure 7a**, when BV molecules are used as surface charge transfer donors for MoS_2 flakes, MoS_2 shows stable n-type doping, characterized by a high electron sheet density of $\approx 1.2 \times 10^{13}$ cm^{-2}. Upon applying a top gate voltage to the device, the device doped with BV molecules exhibits a shifted transfer characteristic curve and a higher on/off current ratio ($\approx 10^6$) at $V_{ds} = 1$ V (Figure 7b).[41]

Similarly, three molecules with dipole moments of different orientations and magnitudes, namely OTS, 3-(trimethoxysilyl)−1-propanamine (APTMS), and trichloro(1H,1H,2H,2H-perfluorooctyl) silane (FOTS), are individually assembled on SiO_2 substrate to form SAMs through covalent bonds and touch the top transferred few-layer MoS_2. By introducing a large positive dipole, the FOTS SAM induces a p-type doping effect on pristine MoS_2 and weakens the n-type doping characteristics of pristine MoS_2 on the substrate. This is reflected in a significant positive threshold voltage shift on the transfer curve of the MoS_2 FET. On the contrary, the reverse dipole moment of APTMS SAM enhances the n-type doping effect of MoS_2, as evidenced by a significant negative threshold voltage shift on the transfer curve. At the same time, the change in carrier density induced by different molecules affects the switching current ratio characteristics of FETs. The switching ratio of FETs with APTMS ($>10^3$) is much higher than that of FOTS (<10), indicating that the doping of the former leads to a higher carrier density of MoS_2.[42] Furthermore, a method for controlled doping by introducing ligand molecules is also proposed.[3] Metal phthalocyanines (MPcs), such as CoPc, MgPc, etc., are initially self-assembled on the surface of MoS_2. Then, pyridines with different functional groups are introduced on the MPc molecules as ligands. The type and position of the functional group respectively determine the orientation and magnitude of the supramolecular dipole moment, thus controlling the doping effect on MoS_2.

In addition to the high carrier density and switching ratio characteristics of FETs, other electrical properties of 2DM can be realized by hybridizing doping effects from different

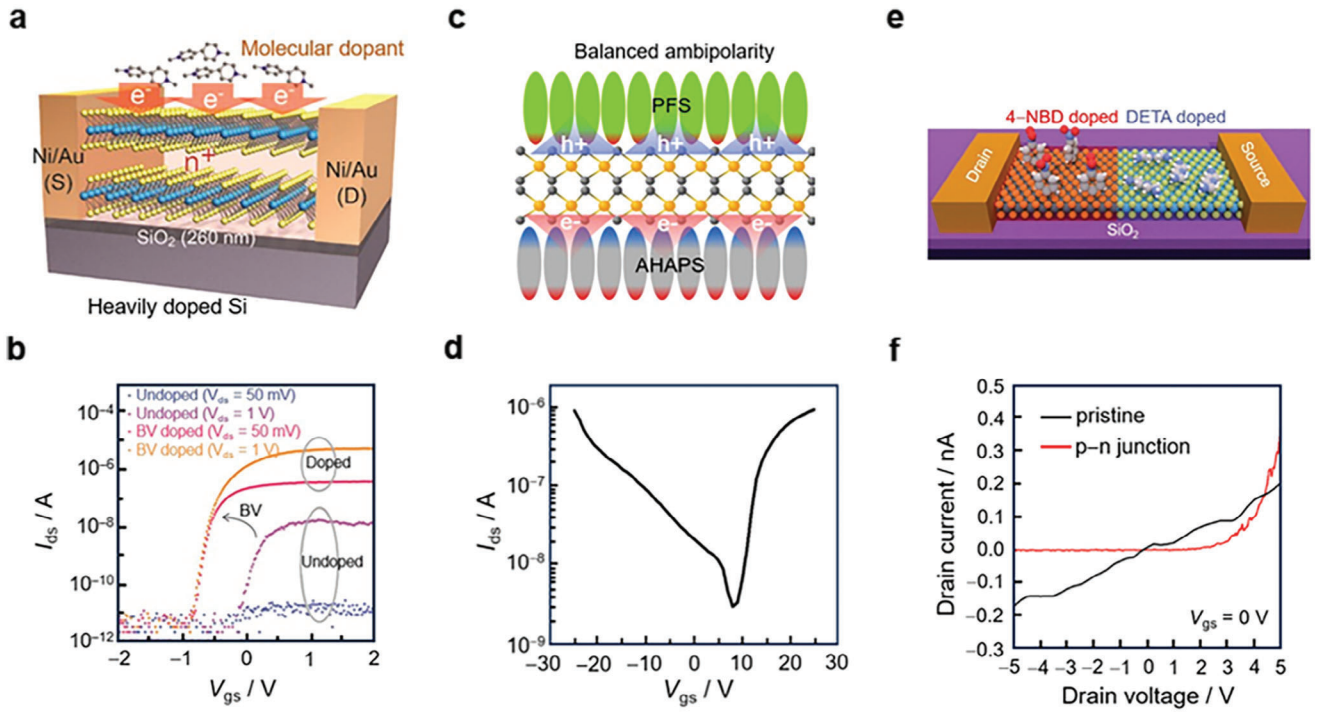

Figure 7. Horizontal conducting devices with "TMD-SAM" heterojunction. a,b) Schematic diagram of horizontal conducting device with unilateral chemical doping on MoS_2 (a) and its corresponding transfer characteristic curves (b). Reproduced with permission.[41a] Copyright 2014, American Chemical Society. c,d) Schematic diagram of horizontal conducting device with asymmetric chemical doping on both sides of WSe_2 (c) and the corresponding transfer characteristic curve (d). Reproduced with permission.[27] Copyright 2019, American Chemical Society. e,f) Schematic diagram of horizontal p-n junction for subregional chemical doping on WSe_2 (e) and its switching performance (f). Reproduced with permission.[45] Copyright 2019, Wiley-VCH.

molecules. WSe_2 is a layered ambipolar semiconductor capable of transferring holes and electrons with a high carrier mobility (μ_h > 200 cm^2 V^{-1} s^{-1} and μ_e > 250 cm^2 V^{-1} s^{-1}, monolayer WSe_2).[43] However, in previous FETs composed of WSe_2, ambipolar transport characteristics could only be observed by applying a high gating electric field or using two different metal electrodes.[44] To fully exploit the ambipolarity of WSe_2 in devices, a new strategy of asymmetric chemical doping is proposed. N-[3- (trimethoxysilyl)propyl]ethylenediamine (AHAPS) molecules are assembled on SiO_2 substrate to induce n-type doping at the bottom of WSe_2, and trichloro(1H,1H,2H,2H-perfluorooctyl)silane (PFS) molecules are assembled on the bilayer WSe_2 to induce p-type doping, as shown in Figure 7c. The transfer curve in Figure 7d demonstrates the ambipolar characteristics of the device, with carrier mobility of similar magnitude (μ_h = 20 cm^2 V^{-1} s^{-1} and μ_e = 5.7 cm^2 V^{-1} s^{-1}) and an on/off current ratio of more than 10^3. However, it should be noted that the same asymmetric functionalization method does not introduce ambipolar properties for monolayer WSe_2. This is because the bilayer WSe_2 allows each layer to have an opposite polarity, making a parallel contribution to the overall charge transport, which cancels out in monolayer WSe_2.[27]

Moreover, a p-n junction on a single WSe_2 grain with a switching function can be realized by spatially controlled chemical doping. As shown in Figure 7e and p-type doping is applied on one side of WSe_2 with 4-nitrobenzenediazonium tetrafluoroborate (4-NBD) and n-type doping with diethylenetriamine (DETA) is applied on the other side of WSe_2. Figure 7f shows the apparent rectification behavior of the doped device (red curve) compared to the I_{ds}–V_{ds} characteristics of the original WSe_2 grain (black curve).[45] The electrical parameters of 2DMs, such as carrier density and working function, can be controlled by selecting suitable dopants and controlling the treatment time and concentration of dopants.[46]

The reversible isomerization of molecules has been extensively studied,[47] and the resulting doping effect is anticipated to be controlled reversibly by switching between the isomers. Recently, an approach for simple and effective controlling the doping effect on the upper surface of 2DM using photoisomeric molecules has been proposed.[48] As the functional unit of the molecule, Azo undergoes a configuration change upon external light irradiation, leading to a redistribution of dipole moments on the surface of MoS_2 and the ability to remotely and effectively control of carrier concentration in MoS_2 using light. This method of using photoisomeric molecules to regulate the chemical doping effects of 2DMs is noteworthy, although the Azo molecules in contact with MoS_2 are multilayered.

Monolayer TMDs have unique optical properties, such as strong PL, strongly bound excitons and charged excitons,[49] and valley polarization,[50] making them promising materials for the development of future optoelectronic devices. When electrons are photoexcited from the valence band to the conduction band in TMDs, they create an electron-hole pair (or exciton), with subsequent relaxation likely from the conduction band to the valence band. The recombination of the electron with the hole induces radiation in a process known as PL. Due to the strong Coulomb

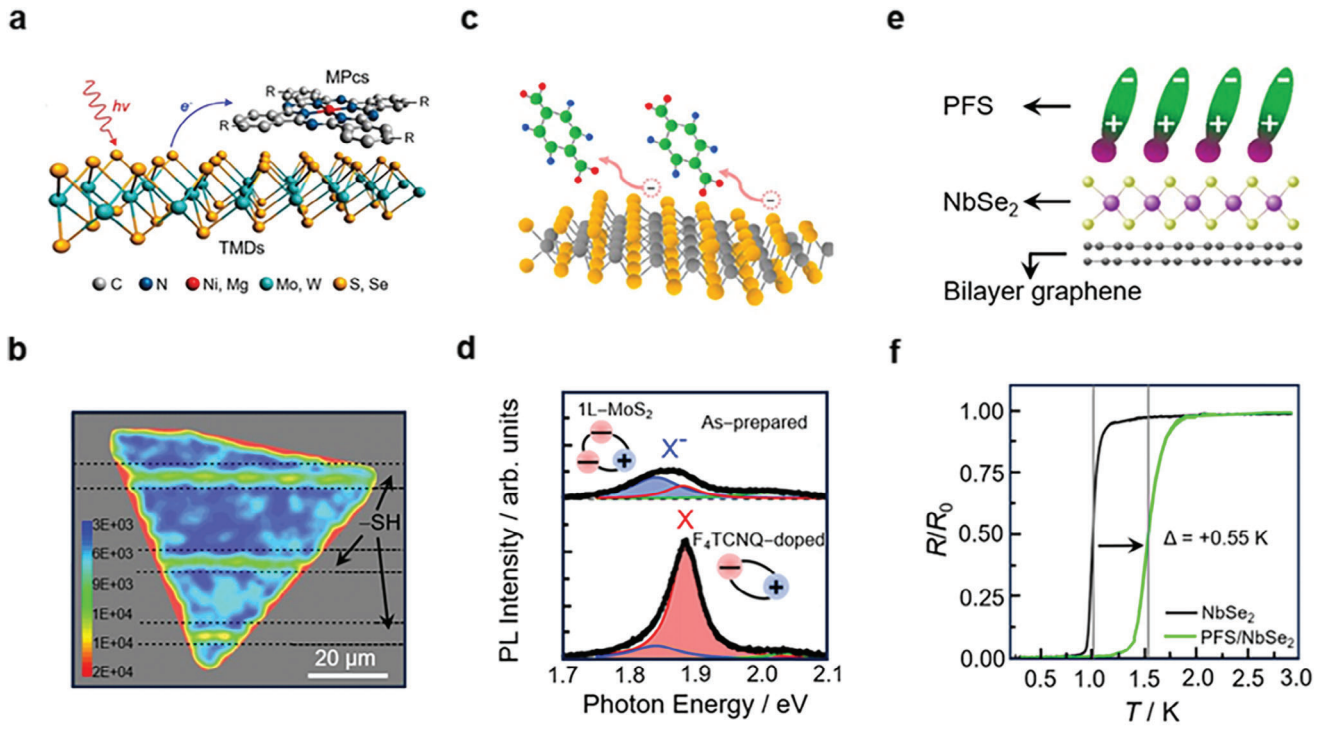

Figure 8. Horizontal conducting devices with "TMD-SAM" heterojunction. a) Schematic presentation of electron transfer process from TMDs to MPcs molecules under illumination. Reproduced with permission.[51] Copyright 2015, American Chemical Society. b) PL intensity map of MoS_2 influenced by the –SH SAM. Reproduced with permission.[60] Copyright 2014, American Chemical Society. c) Schematic diagram of p-type doping on MoS_2 by F_4TCNQ SAM. d) PL intensity of the pristine (upper) MoS_2 and after doping with F_4TCNQ SAM (lower). Reproduced with permission.[28b] Copyright 2013, American Chemical Society. e) Schematic diagram of the method for manipulating the T_c of $NbSe_2$. f) Normalized R– T measurements of $NbSe_2$ with and without PFS SAM. Reproduced with permission.[58] Copyright 2020, American Chemical Society.

interaction in atomically thin TMDs, the exciton binding energy is 0.6 eV for MoS_2 and 0.37 eV for WSe_2.[49a,c]

The optical properties of TMDs can be regulated through charge transfer from TMDs to molecules.[51] As shown in **Figure** 8a, the adsorption of MPc molecules on the surface of MoS_2 leads to the transfer of electrons excited by incident light to the molecules, thereby inhibiting the exciton recombination of MoS_2 itself. It is important to note that this requires the selection of TMDs and molecules with matching energy levels. For example, NiPc molecules adsorbed on different TMDs have different effects on the regulation of PL of TMDs. While NiPc molecules cannot inhibit the PL properties of monolayer MoS_2, they can inhibit those of monolayer WSe_2 and $MoSe_2$. When choosing MgPc molecules, only the PL properties of WSe_2 can be inhibited. This is due to the transfer of excited electrons to the molecular energy level when the reduction potential of molecules is below the CBM of the single-layer TMDs, which reduces the recombination of excited electrons and holes in the valence band and thus inhibits the PL properties of TMDs. Conversely, if the reduction potential of molecules is higher than the CBM of the TMDs, the excited electrons cannot be transferred to the molecule, and thus do not affect the PL properties. Notably, the inhibitory effect of MPc molecules on the PL properties disappears upon the removal of MPc molecules, allowing for flexible and reversible tuning of PL properties of TMDs. In Figure 8b, the PL intensity diagram of MoS_2 in a SiO_2-monolayer MoS_2 heterojunction with– SH as the end group of the SAM is presented. The dashed lines distinguish the underlying– SH patterns, highlighting the enhancement of PL intensity associated with dipole moment and charge transport brought by the SAM. Moreover, the PL intensity decreases as the temperature increases, which is thought to be due to the thermal activation of nonradiative recombination centers.

The interaction between the exciton and the carrier leads to the formation of a multibody bound state, such as the charged exciton (trion).[49a] Therefore, it is expected that the optical properties of TMDs can be regulated by adjusting the density and proportion of excitons and trions. Specifically, the change of carrier density through chemical doping is an effective means to regulate PL properties, which has been extensively studied.[3,27,48,52] As shown in Figure 8c, the assembly of 2,3,5,6-tetrafluoro-7,7,8,8-tetracyanoquinodimethane (F_4TCNQ) molecules on the surface of a monolayer MoS_2 absorbs electrons of MoS_2, resulting in a p-type doping effect. Furthermore, the PL spectra of single layers of MoS_2, with or without F_4TCNQ molecules, demonstrate the important role of carrier doping in regulating PL properties from a perspective of mechanism, as shown in Figure 8d.[28b] In the case of monolayer MoS_2, two conventional peaks indicating exciton formation are observed near 1.92 eV (A exciton) and 2.07 eV (B exciton), respectively. Moreover, peak A includes an X^- trion peak composed of two electrons and one hole (blue line) and an X exciton peak composed of one electron and one hole (red line),

which are consistent with previous research results.[52,53] After p-type doping, the PL intensity of A and B excitons increases, with the X exciton peak intensity (red line) higher than the X^- trion peak intensity (blue line), suggesting that F_4TCNQ-induced p-type doping increases exciton radiative recombination.

In contrast, when nicotinamide adenine dinucleotide (NADH) molecules are used for n-type doping of MoS_2, the PL peak intensity decreases, and the peak shifts to the X^- trion peak compared with undoped MoS_2. This indicates that the enhancement of electron density increases the number of trions, thereby reducing the radiation recombination of excitons. In fact, molecular doping not only regulates the optical properties of TMDs, but also provides a new method for controlling the performance of TMDs-based photoelectric devices. A decrease in PL intensity means a reduction in carrier recombination, which leads to an increase in photocurrent, and vice versa.[54] For example, in APTES doped MoS_2 photodetectors, n-type doping leads to a reduction in the PL intensity. The optical responsiveness of the device is improved by a factor of ≈26.4 (from 219 to 5.75×10^3 A W^{-1}), which is much higher than previously reported TMDs photodetectors.[52,55] Therefore, the selection of appropriate molecular doping plays an important role in improving the performance of TMDs-based optoelectronic devices.

Apart from the regulation of electrical and optical properties, the contact of SAMs with 2DMs also has implications for the intrinsic physical characteristics of 2DMs, including superconductivity. The transition of 2DM $NbSe_2$ to a superconducting state occurs below the critical temperature (T_C). Notably, in SAMs, the T_C is lower (≈1 K) compared to that in bulk crystals (≈7 K).[56] Manipulating the low-temperature superconducting state on the surface of $NbSe_2$ is achievable through the use of molecules, such as paramagnetic and non-magnetic chiral molecules.[57] In addition, molecules with opposite dipoles can cause opposite shifts in T_C.[58] AHAPS and PFS molecules, each with permanent dipoles, are assembled on a single layer of $NbSe_2$ to create 2DM-SAM heterojunctions (Figure 8e). The normalized R and T measurements of $NbSe_2$ before and after the assembly of PFS molecules are shown in Figure 8f, where resistances are normalized to the value of the resistance state above T_C (R_0), and T_C represents the temperature corresponding to $R_0/2$. Relative to the T_C of $NbSe_2$ (1.0 ± 0.1 K), the T_C of PFS-assembled $NbSe_2$ increases to 1.55 K, while that of AHAPS-assembled $NbSe_2$ decreases to below 0.29 K. The change of carrier density induced by different molecular dipoles influences the original electron–phonon interaction, which is closely associated with the formation of Cooper pairs and the superconducting state.[59]

3.2. 2DM-SAM in Contact with Chemical/Biological Solution

While the regulation of properties in most horizontal 2DM-SAM heterojunctions typically occurs under vacuum or air conditions, it is noteworthy that regulation in a solution also plays a crucial role.[61] Ionic liquid, with a higher electric field than that of traditional back-gate, provides a new approach for effectively regulating horizontal 2DM-SAM devices.[62] Specifically, the diethylmethyl(2-methoxyethyl)ammonium bis(trifluoromethylsulfonyl)imide (DEME-TFSI) ionic liquid is an unconventional electrolyte with highly repeatable electrochemical behavior.[63] As shown in **Figure 9**a, Fc is a typical electrochemical switchable molecular unit that can be attached to the end of an alkyl thiol and then assembled on the surface of MoS_2 through the sulfur vacancy of MoS_2. DEME-TFSI is dripped onto the 2DM-SAM devices, and a Pt wire is immersed into the ionic liquid as a top gate electrode. The two-electrode electrochemical cell involves MoS_2 and Pt wires as working and counter electrodes, respectively, using DEME-TFSI to establish an electrolyte environment for the redox reaction of Fc. The voltage applied to the top gate electrode creates an EDL at the interfaces between ionic liquid and monolayer MoS_2, as well as the ionic liquid and the gate electrode, thereby regulating the redox state of the SAM and the doping effect of SAM on MoS_2. The device transfer curves under back-gate control corresponding to Fc units in different states are shown in Figure 9b, which achieve the reversible regulation of the doping effect of SAM through electrochemical means.

With an extraordinarily high surface-to-volume ratio, atomically thin 2DMs are highly responsive to their surroundings, allowing for easy modification by external inputs.[48] Meanwhile, molecules with rich structures and functions provide a broad and stable platform for 2DMs to communicate with their surroundings. Therefore, the 2DM-SAM heterojunction represents a viable protocol for developing functional devices suitable for sensing applications. A design of nitric oxide (NO) sensors based on hemin-functionalized Gr FET has been developed for application in biological systems with excellent selectivity and sensitivity.[8] As shown in Figure 9c, hemin molecules can be immobilized on Gr by π– π stacking and can selectively bind to NO, which ensures high sensitivity and specific detection of NO. The detection result of NO in physiological solutions such as cell culture media or real biological samples like fetal bovine serum can be inferred from the conductance value of Gr, influenced by the doping effect induced before and after the specific binding of NO. As shown in Figure 9d, the introduction of interfering chemicals, including oxygen and hydrogen peroxide, does not cause a significant change in conductance. However, upon the addition of 1 nM NO, a substantial change in conductance can be observed, and higher concentrations of NO result in a more pronounced change in conductance.

Beyond the specific detection of small molecules, functionalized 2DMs enable the detection of biological macromolecules, which is beneficial for the study of immune responses in organisms and disease treatments. For instance, a biosensor for the rapid and sensitive detection of severe acute respiratory syndrome coronavirus 2 (SARS-CoV-2) in physiological solutions is achieved by functionalizing monolayer WSe_2 with SARS-CoV-2 spike protein antibodies, based on the specific binding of the viral antigen to the corresponding antibody.[64] In Figure 9e and 11-mercaptoundecanoic acid (MUA) effectively binds the SARS-CoV-2 antibody to WSe_2. The results indicate that the specific binding of SARS-CoV-2 spike proteins and antibodies resulted in an increase in the current of WSe_2 FETs (Figure 9f). Overall, the specific molecular interactions facilitate the development of sensitive and rapidly responsive biochemical sensors through the appropriate functionalization of 2DM-SAM.

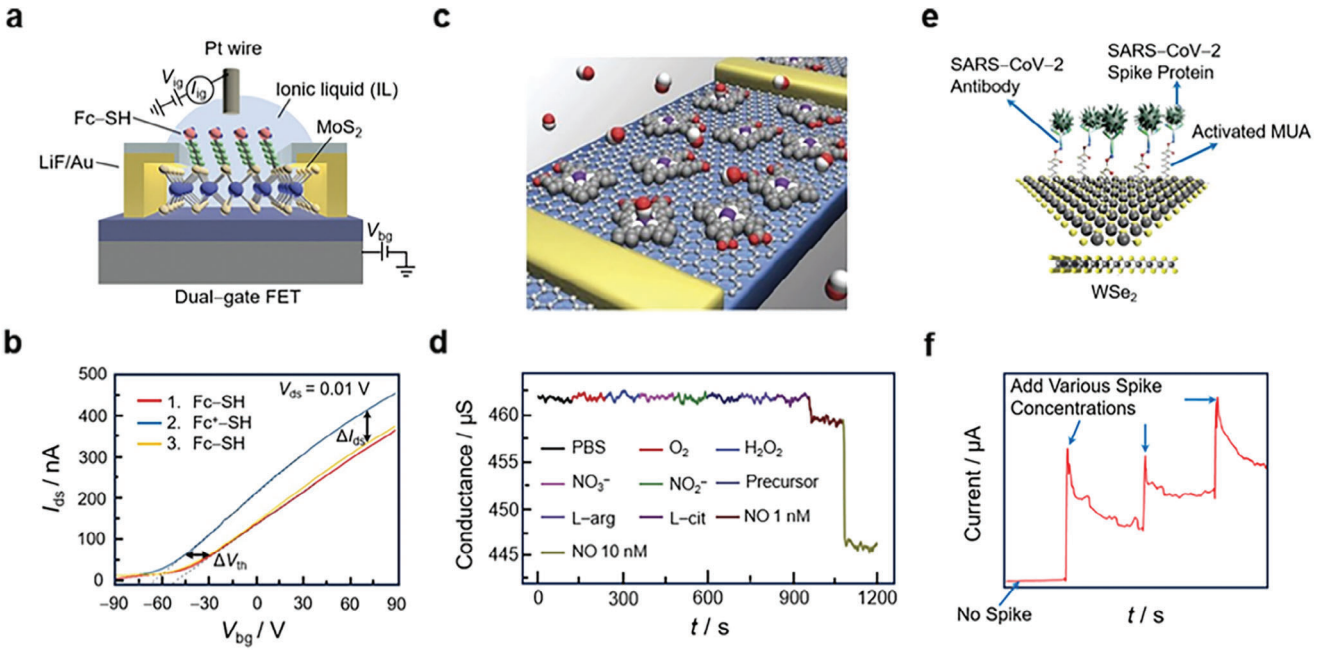

Figure 9. Horizontal conducting devices with "2DM-SAM" heterojunction in contact with solution. a) Schematic diagram of the dual-gated MoS_2-Fc-SH SAM device. b) Back-gate transfer characteristic curves of the MoS_2-SAM device with different Fc-SH electrochemical states under ionic liquid-gate regulation. Reproduced with permission.[61] Copyright 2020, Wiley-VCH. c) Schematic diagram of Gr-hemin SAM device that selectively responds to the NO molecule. d) Conductance changes upon the sequential addition of a series of control solutions and NO solutions. Reproduced with permission.[8] Copyright 2013, Springer Nature. e) Schematic diagram of the SARS-CoV-2 sensor based on WSe_2-SAM. f) Electrical measurement of the sensor with the addition of the SARS-CoV-2 spike protein. Reproduced with permission.[64] Copyright 2021, American Chemical Society.

3.3. 2DM-SAM in Contact with Metal

While 2D semiconductor materials have attracted considerable attention for their unique electrical and optical properties, the development of high-performance devices based on these materials has been hampered by issues such as the Schottky barrier and large contact resistance arising from direct contact with metal electrodes.[65] Several strategies have been proposed to reduce the contact resistance at the metal-2DM interface, including high-temperature annealing,[66] additional steps involving the introduction of graphene or hexagonal boron nitride as an interlayer,[67] and the selection of metals with low work functions to align with the conduction band of 2DMs.[68] The use of SAMs to functionalize 2DMs has been proposed as a productive and alternative approach to improve contact performance.[69]

As shown in **Figure 10a**, perfluorodecanethiol (PFDT) molecules can be selectively adsorbed by sulfur vacancies on the surface of MoS_2 through vapor deposition, which introduces an additional thin tunneling path in the contact region of Au and MoS_2. For the Au-MoS_2 interface without molecular treatment, the carrier injection characteristics are determined by the Schottky barrier as well as the tunneling barrier caused by the vdW gap naturally formed between the metal and the 2DM. The main carrier injection mechanism is thermionic emission, which requires sufficient activation energy to overcome the barrier between Au and MoS_2. Therefore, for untreated MoS_2 FETs, I_{ds} tends to increase with rising temperature. In contrast, for the thiol-treated Au-MoS_2 interface, the combination of thiol molecules and sulfur vacancies creates a tunneling path with a lower thin barrier at the interface, hindering the Au-MoS_2 interaction and removing the interface states (sulfur vacancies) responsible for Fermi level pinning.[69,70] Consequently, carriers can be injected from Au electrode to MoS_2 via field emission even with much lower activation energy (Figure 10b). The I_{ds} of the thiol-treated MoS_2 FETs is essentially maintained as the temperature increases, as shown in Figure 10c. After PFDT treatment, the normalized contact resistance of the device is reduced from ≈175.5 to ≈67.7 kΩ μm. Meanwhile, the output current increases from ≈20 μA to over 30 μA (at $T = 80$ K, $V_{gs} = 40$ V, and $V_{ds} = 3$ V). Overall, the introduction of thiol molecules induces a transition from Schottky contact to Ohmic contact behavior, thereby increasing the tunneling current.

From another perspective, in addition to the introduction of thin tunneling barriers, molecular assembly between the metal and the 2DM can also lead to the reduction of the metal work function or the increase of the 2DM Fermi level. This is beneficial as it aligns the energy levels of the metal electrode and the 2DM, thus lowering the barrier.[5,71] An approach has been proposed to improve the contact performance of the Au-MoS_2 interface by adjusting the work function of the metal through molecular monolayer assembly (Figure 10d). In this approach, molecules are pre-assembled onto the metal electrode via the Au– S bond, following which MoS_2 is transferred onto the SAM. Figure 10e shows the work function range of Au after the assembly of different molecules (BP0-down, BP0, and BP0-up) and the electron affinity range of MoS_2 flakes, assuming vacuum level alignment.[71,72] Among them, the electrodes assembled

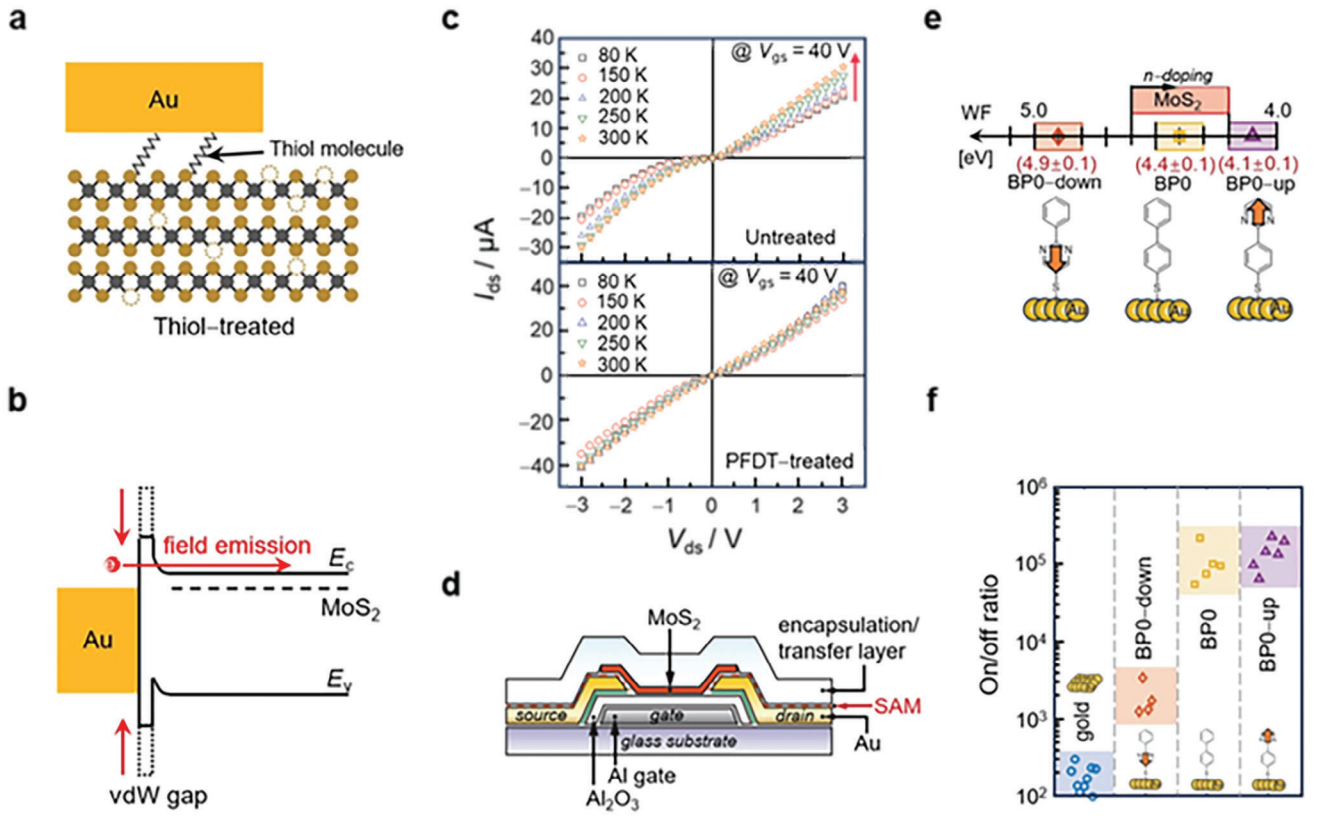

Figure 10. Horizontal conducting devices with "2DM-SAM" heterojunction in contact with metal. a) Structure of thiol-treated MoS_2 in contact with Au electrode. b) Energy band diagram of the contact between thiol-treated MoS_2 and the Au electrode. c) Temperature dependent I_{ds}–V_{ds} output curves of the untreated and PFDT-treated MoS_2 device. Reproduced with permission.[69] Copyright 2018, Wiley-VCH. d) Structure of the SAM-treated MoS_2 device in contact with the gold electrode. e) Work function range of SAM-treated electrodes compared to the electron affinity range of MoS_2 flakes. f) On/off ratio as a function of electrodes treated by different SAMs. Reproduced with permission.[71] Copyright 2020, Wiley-VCH.

with BP0 and BP0-up exhibit work function closer to the electron affinity range of MoS_2 flakes, which allows both interfaces to exhibit low contact resistance during electron injection, both from the source electrode to MoS_2 and from MoS_2 to the drain electrode. For the Au/BP0/MoS_2 heterojunction, the output current (I_d) is ≈1.6 μA at $V = 1$ V. In contrast, for the Au/MoS_2 heterojunction with a similar current transmission length, I_d is only ≈25 nA. The introduction of the BP0 SAM significantly reduces the contact resistance in MoS_2-based FETs compared to unmodified electrodes (13.56 vs 0.01 kΩ cm), leading to an on/off ratio increase of more than two orders of magnitude (Figure 10f).

3.4. Horizontal Devices Relying on SAM for Charge Transport

In most horizontal devices with 2DM-SAM heterojunctions, the 2DM is typically used as the conduction path and metal is used as the electrode. However, this setup tends to underutilize the rich molecular properties in enhancing device performance. Moreover, the high energy barrier between the metal and the 2DM limits the development of high-performance FETs, which are characterized by characteristics such as high mobility and a high switching ratio. A novel horizontal device employing a 2DM-SAM heterojunction, where the SAM acts as the conduction path and 2DM as electrode, has been proposed.[73] As shown in **Figure 11a**, monolayers of copper phthalocyanine (CuPc) molecules with a face-to-face π– π packing conformation strongly interact with the monolayer Gr electrodes in two dimensions, giving rise to back-gate regulated molecular FETs. The Gr nanogap is crafted by the oxidative cutting of individual Gr sheets through an ultrafine lithographic process and precise oxygen plasma etching. The electrical characteristics of Gr before and after oxidative cutting, alongside the AFM image following the assembly of the SAM are shown in Figure 11b. The current of Gr after cutting is nearly zero. Compared with metal electrodes, due to the low work function (4.7 to 4.9 eV) of Gr, there is a favorable interface contact and a low injection barrier between Gr and the SAM.[74] This results in both high carrier mobility (up to 0.04 $cm^2 V^{-1} s^{-1}$) and a high on/off current ratio (>10^6) for the FETs. Furthermore, the photoactive properties of CuPc molecules are fully realized. Figure 11c demonstrates that the photoelectric response characteristics of the device are consistent with the UV/Vis absorption spectra of corresponding CuPc films. The photoelectric response can occur in a SAM with a thickness of only 1.3 nm, thanks to the effective charge injection with small bias allowed by the low injection barrier, which avoids harmful charge recombination under light irradiation and prevents the quenching effect by the environments.

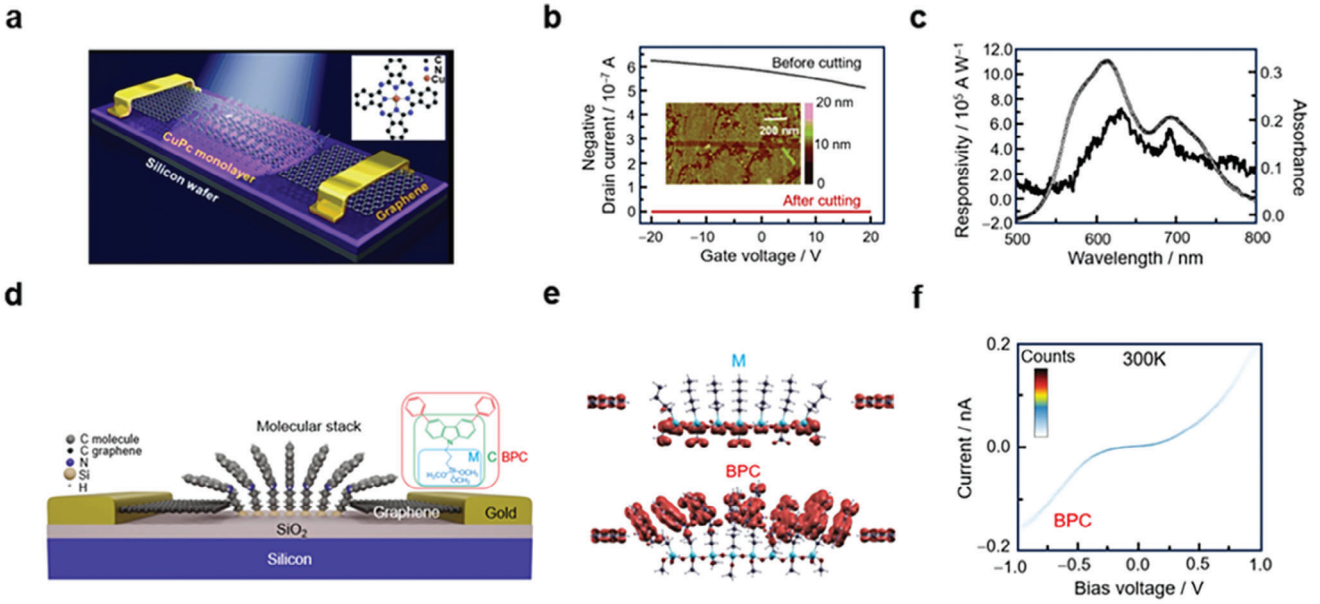

Figure 11. Horizontal devices relying on SAM for charge transport. a) Structure of the CuPc SAM transistor device with Gr as electrodes. b) I_{ds}– V_{gs} transfer characteristic curves of Gr before and after oxidative cutting. c) The wavelength-dependent spectrum (black line) and the UV/Vis absorption spectrum (gray circles) of CuPc thin films. Reproduced with permission.[73] Copyright 2010, Wiley-VCH. d) Schematic diagram of a device containing a π– π stacked SAM that fulfils the nanogap between Gr electrodes. e) Local state density of the M/BPC SAM and Gr electrodes heterojunctions. f) *I*–*V* plots of the BPC device. Reproduced with permission.[75] Copyright 2019, Springer Nature.

In addition, as shown in Figure 11d, the covalent connection of the molecular terminal groups to the SiO_2 substrate ensures the overall mechanical stability of these horizontal devices. Furthermore, the π– π packing between BPC molecules gives rise to a uniform and compact SAM, contributing to the high electronic stability of the charge transport process in devices.[75] As shown in Figure 11e, the wave function extends over the biphenyl N-carbazole groups for the BPC SAM, whereas for the M SAM, no delocalized orbitals are formed, and transport occurs via the poorly conducting silane groups. This demonstrates the critical role of the π– π stacking head group in transport and rationalizes the fact that the current of the BPC SAM (Figure 11f) is much higher than that of the M SAM observed in the experiment.

4. 2DM-SAM Hybrid Superlattice Devices

Molecular intercalated 2DMs refers to stable superlattice structures formed by the interaction between guest molecules and the host 2DMs, which allows the insertion of molecules into the interlayer voids of 2DMs. The guest molecules discussed in this section include not only neutral molecules but also emphasize organic cations, especially those derived from ammonium salts. The structural modification of 2DMs through molecular intercalation often results in changes to their properties, such as electrical conductivity, thermal conductivity, magnetism, etc. Moreover, the incorporation of different 2DMs with molecular intercalation in devices holds the potential to achieve specific functionalities.

4.1. Construction of 2DM-SAM Hybrid Superlattices

There are many methods to obtain intercalated 2DMs, including the vapor transport method,[76] solvent-based intercalation,[77] electrochemical intercalation,[78] and artificial assembly.[79] Among these, electrochemical intercalation stands out a mild, efficient, and controllable strategy for achieving intercalation.[80] The construction of molecular films through electrochemical methods mainly relies on the electrostatic interactions between 2DM electrodes and charged molecules. The resulting heterostructures with an alternating arrangement of 2DM layers and molecular films are referred to as 2DM-SAM hybrid superlattices. It is important to note that these hybrid superlattices are not as uniform as those produced by self-assembly techniques. In these hybrid superlattice structures, the molecular films between adjacent 2DM layers are not necessarily monolayer and can consist of several layers.

Figure 12a shows a BP superlattice device with molecular intercalation prepared through electrochemical intercalation. Briefly, molecular intercalation of BP with cetyltrimethylammonium bromide (CTAB) molecules takes place in a three-electrode electrochemical cell, with Pt used as the counter electrode, Ag/AgCl as the reference electrode, and the organic cations CTA^+ being intercalated into the vdW gap of the BP cathode. Figure 12b simulates the structure of monolayer phosphorene molecular superlattices (MPMS) after intercalation, allowing the extraction of key intrinsic properties of the single layer of BP. Moreover, when the device is placed under a Raman/PL microscope, the intercalation process can be monitored by both the current and Raman/PL spectra in situ.[78a]

4.2. Properties of 2DM-SAM Hybrid Superlattices

Recently, there has been a growing interest in the distinctive properties of organic cationic intercalation 2DMs obtained by

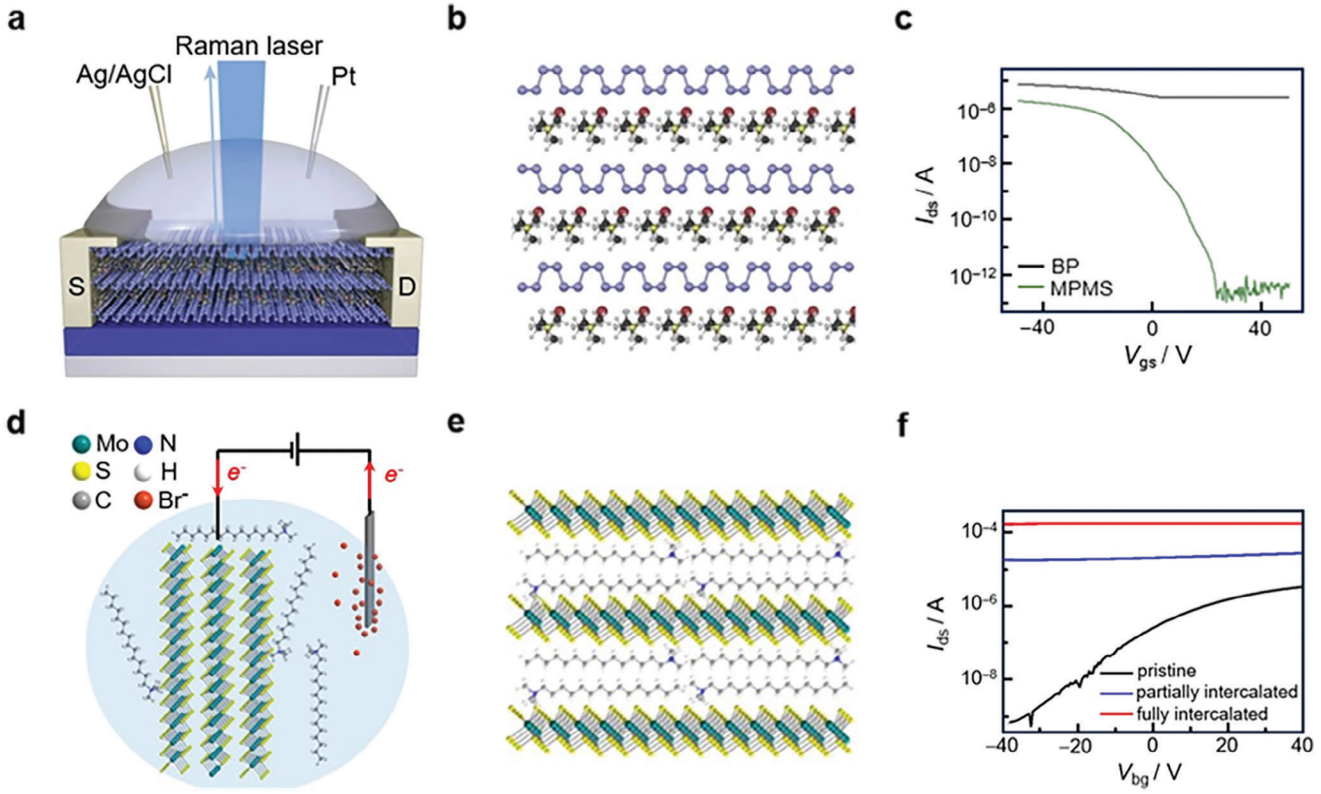

Figure 12. 2DM-SAM hybrid superlattices. a) Schematic presentation of the electrochemical-optical measurement platform for BP intercalation. b) Cross sectional view of the simulated atomic structure of MPMS. c) I_{ds}– V_{gs} transfer characteristic curves of BP and MPMS devices. Reproduced with permission.[78a] Copyright 2018, Macmillan Publishers Limited, part of Springer Nature. d) Schematic illustration of MoS_2 intercalated with CTA^+ organic cations. e) Structure of the MoS_2-CTA^+ hybrid superlattice. f) I_{ds}– V_{gs} transfer characteristic curves of the MoS_2 device at different stages of CTA^+ intercalation. Reproduced with permission.[81] Copyright 2019, American Chemical Society.

electrochemical intercalation processes, showing their potential for building devices with excellent electrical performance. For example, as shown in Figure 12b, the MPMS of CTA^+ intercalation increases the bandgap width of monolayer BP from 1.94 to 2.13 eV, thereby changing the semiconductor properties of BP.[78a] Figure 12c shows the transfer curves of both BP and MPMS FETs before and after intercalation, wherein the on/off current ratio of MPMS FETs exceeding 10^7, significantly enhancing the switching performance of the device. Similarly, as shown in Figure 12d, molecular intercalation of MoS_2 with CTA^+ takes place based on the principle of electrochemical intercalation, wherein the organic cations CTA^+ are inserted into the van der Waals gap of the MoS_2 cathode. Concurrently, the anions accumulate near the counter electrode, forming the superlattice structure as shown in Figure 12e.[81] The intercalation of CTA^+ induces a phase transition of MoS_2, transforming from a semiconductor to a metal, resulting in a significant increase in conductivity (>5 orders of magnitude). The transfer curves at different stages during the CTA^+ intercalation processes are shown in Figure 12f, from the pristine MoS_2 with n-type doping characteristic to the partially intercalated MoS_2 with small gate regulation, and finally to the superlattice with almost no gate regulation. Different molecular intercalation can manifest different semiconductor properties. For example, in contrast to the previous case, the MoS_2 superlattice intercalation with tera-heptyl-ammonium cation (THA^+) maintains a semiconducting 2H-MoS_2 phase.

In addition to regulating the semiconductor characteristics of 2DMs, molecular intercalation can be applied to modulate their magnetic properties. Notably, electrochemical intercalation of tetrabutyl ammonium (TBA^+) cations has been reported to induce the conversion of $Cr_2Ge_2Te_6$ from a ferromagnetic semiconductor to a ferromagnetic metal, due to the electron doping effect of intercalation.[82] This intercalation-induced changes in the magnetic coupling mechanism significantly raises the Curie temperature of $Cr_2Ge_2Te_6$ from 67 to 208 K, accompanied by a change in the direction of the magnetic easy axis. Furthermore, a novel spintronic device has been constructed based on the chiral molecular intercalation 2DM superlattice and a magnetic electrode.[4] **Figure 13a** shows the formation of right-handed (R-) and left-handed (S-) chiral molecular intercalation superlattices (CMIS) by chiral molecular intercalation of TaS_2, respectively. The CMIS, along with an Au electrode and a ferromagnet Cr_3Te_4 electrode then establishes a spin tunneling junction (STJ). When charge is transported through specific chiral molecules or structures, an electron spin polarization associated with molecular chirality occurs, and this phenomenon is known as the chiral-induced

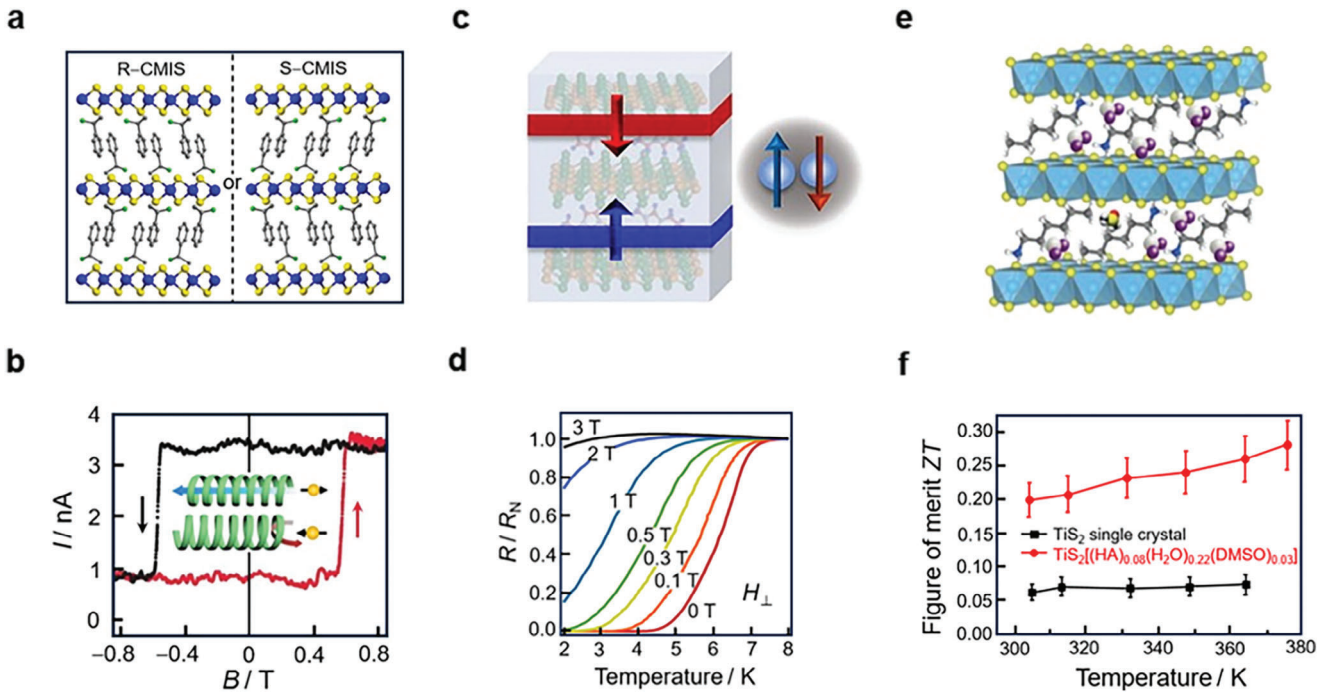

Figure 13. 2DM-SAM hybrid superlattices. a) R-CMIS and S-CMIS with alternating layers of TaS_2 and chiral molecules. b) Magnetic-field-dependent tunneling current measured in the S-CMIS with CISS effect. Reproduced with permission.[4] Copyright 2022, Springer Nature. c) Schematic presentation of the emergence of superconducting weak topological insulators from type-II Weyl fermion in bulk $MoTe_2$ through ion intercalation. d) Resistance of the $MoTe_2$-molecular monolayer superlattice under different magnetic fields. Reproduced with permission.[84c] Copyright 2019, Science China Press and Elsevier. e) Schematic diagram of the TiS_2-based hybrid superlattice structure. f) In-plane ZT of TiS_2 single crystal and TiS_2-based hybrid superlattice. Reproduced with permission.[85] Copyright 2015, Macmillan Publishers Limited.

spin selectivity (CISS) (Figure 13b). A bidirectional magnetic field scan of the S-CMIS STJ at a constant bias voltage shows typical characteristics of STJs. The CISS effect of chiral molecules can lead to asymmetric spin tunneling probability for carriers with different spin polarization directions. During the field sweep scan, when the magnetic field surpasses the coercive field of Cr_3Te_4, there is an abrupt switch in the out-of-plane ferromagnetic order of Cr_3Te_4, leading to an instantaneous change in the spin polarization direction of carriers, and subsequently causing a sudden shift in the tunneling probability through the CMIS. Notably, the R-CMIS STJ displays the I- B curve with an opposite trend. This CMIS STJ, with a distinct chirality-dependent tunneling current, demonstrates a magnetoresistance of over 300% and the spin polarizability of more than 60%. The versatility of layered 2DMs and customizable chiral molecular structures opens up possibilities for designing and integrating novel spintronic devices.

Organic cations intercalation provides a new pathway for enhancing the superconductivity of superconducting materials. For example, a single layer of WTe_2 exhibits emergent superconductivity with $T_c \approx 0.82$ K, which is absent in bulk crystals.[83] The intercalation of organic cations induces a reduction in the interlayer coupling of WTe_2 single crystals, transforming them from a 3D type-II Weyl semimetal to a 3D weak topological insulator (Figure 13c). This results in a significant enhancement of superconductivity ($T_c \approx 2.3$ K).[84] The improved superconductivity is attributed to the increase in the density of states near the Fermi level, brought about by the introduction of organic cations that disrupt the balance of electrons and holes. Similarly, organic cationic intercalated $MoTe_2$ crystals exhibit enhanced superconductivity, as evidenced by an increase in T_c increasing from 0.25 to 7.0 K. Furthermore, the resistance of intercalated $MoTe_2$ under different out-of-plane magnetic fields, as shown in Figure 13d, demonstrates the tunability of superconductivity by magnetic fields.

The $TiS_2[(HA)_x(H_2O)_y(DMSO)_z]$ hybrid superlattice, characterized by a high thermoelectric figure of merit (ZT), is formed through the electrochemical intercalation of hexylammonium (HA) ions with TiS_2 and subsequent solvent exchange reactions (Figure 13e).[85] The coupling between the inorganic layers and the organic layers resulting from the intercalation of organic cations, as well as the deformation of the superlattice, disrupt photon transport in the plane direction and increase the phonon scattering at the interface and reduces the thermal conductivity of TiS_2. At the same time, the intercalation of organic cations introduces additional stable electrons to the inorganic layer, which improves the electrical conductivity of TiS_2. Overall, the increase of electrical conductivity and the decrease of thermal conductivity contribute to an elevated ZT value. This suggests that the intercalation of organic ions has the potential to facilitate more efficient thermoelectric conversion of certain thermoelectric materials. Furthermore, with the rise in temperature, ZT reaches 0.28 at 373 K, as shown in Figure 13f, which is close to that of the most promising p-type organic material PEDOT-PSS.[86]

5. Conclusion

In this review, we have discussed the latest development in electronic and optoelectronic devices based on 2DM-SAM heterojunctions. The fabrication of devices with superior material properties has been achieved through the hybridization of various SAMs and 2DMs with rich chemical and physical properties. In the design of vertical tunneling devices, the employment of 2DM electrodes and external control means can fully exert the properties of molecular SAMs, which is crucial for understanding the working mechanisms of 2DM-SAM heterojunction devices. For horizontal conducting devices, the functional SAMs regulate the properties of 2DMs, realizing the high performance of 2DM-SAM devices. For the 2DM-SAM hybrid superlattices, the intercalation of SAMs with thickness comparable to that of monolayer 2DM changes the basic physical properties of the 2DM crystals. On this basis, devices with high performance or new functions have been realized.

Research in this field is still in its early stages, and there is still a lot of works to be explored. For the preparation process, it is necessary to develop more stable, controllable, and atomically accurate methods of molecular self-assembly on 2D materials, which is critical to improving the yield and stability of fabricated devices. For instance, atomic-level precise covalent assembly processes need to be developed to assemble molecular monolayers onto BP, TMDs, and other 2D materials. To realize the application of 2DM-SAM heterojunctions, it is necessary to explore the new functions and working mechanisms of the corresponding devices, especially the switching, field effect, and magnetic characteristics. In addition, the high-density integration of the devices is also key to real-world applications. New integration strategies need to be developed, especially with crossbar architectures, which are essential to realize their applications in sensing, computing, and information storage. Overall, close collaborations between chemists, physicists, materials scientists, and engineers are needed to advance this field and enable practical applications of 2D organic-inorganic heterostructures.

Acknowledgements

The authors acknowledge primary financial supports from the National Key R&D Program of China (2021YFA1200102, 2021YFA1200101, and 2022YFE0128700), the National Natural Science Foundation of China (22173050, 22150013, 21727806, and 21933001), and the Natural Science Foundation of Beijing (2222009).

Conflict of Interest

The authors declare no conflict of interest.

Keywords

2D material, field-effect transistor, graphene, heterojunction, self-assembled monolayer, transition metal dichalcogenide, van der Waals

Received: April 10, 2024
Revised: June 11, 2024
Published online:

[1] J. Li, J. Wierzbowski, Ö. Ceylan, J. Klein, F. Nisic, T. L. Anh, F. Meggendorfer, C. A. Palma, C. Dragonetti, J. V. Barth, J. J. Finley, E. Margapoti, *Appl. Phys. Lett.* **2014**, *105*, 241116.
[2] C. Jia, I. M. Grace, P. Wang, A. Almeshal, Z. Huang, Y. Wang, P. Chen, L. Wang, J. Zhou, Z. Feng, Z. Zhao, Y. Huang, C. J. Lambert, X. Duan, *Chem* **2020**, *6*, 1172.
[3] Y. Wang, S. M. Gali, A. Slassi, D. Beljonne, P. Samorì, *Adv. Funct. Mater.* **2020**, *30*, 2002846.
[4] Q. Qian, H. Ren, J. Zhou, Z. Wan, J. Zhou, X. Yan, J. Cai, P. Wang, B. Li, Z. Sofer, B. Li, X. Duan, X. Pan, Y. Huang, X. Duan, *Nature* **2022**, *606*, 902
[5] D. Yue, C. Kim, K. Y. Lee, W. J. Yoo, *Adv. Funct. Mater.* **2019**, *29*, 1807338.
[6] S. Seo, M. Min, S. M. Lee, H. Lee, *Nat. Commun.* **2013**, *4*, 1920.
[7] N. Nerngchamnong, L. Yuan, D. C. Qi, J. Li, D. Thompson, C. A. Nijhuis, *Nat. Nanotechnol.* **2013**, *8*, 113.
[8] S. Jiang, R. Cheng, X. Wang, T. Xue, Y. Liu, A. Nel, Y. Huang, X. Duan, *Nat. Commun.* **2013**, *4*, 2225.
[9] a) P. Song, S. Guerin, S. J. R. Tan, H. V. Annadata, X. Yu, M. Scully, Y. M. Han, M. Roemer, K. P. Loh, D. Thompson, C. A. Nijhuis, *Adv. Mater.* **2018**, *30*, 1706322; b) P. Song, C. S. S. Sangeeth, D. Thompson, W. Du, K. P. Loh, C. A. Nijhuis, *Adv. Mater.* **2015**, *28*, 631.
[10] a) M. Famili, C. Jia, X. Liu, P. Wang, I. M. Grace, J. Guo, Y. Liu, Z. Feng, Y. Wang, Z. Zhao, S. Decurtins, R. Häner, Y. Huang, S. X. Liu, C. J. Lambert, X. Duan, *Chem* **2019**, *5*, 474; b) C. C. Jia, M. Famili, M. Carlotti, Y. Liu, P. Q. Wang, I. M. Grace, Z. Y. Feng, Y. L. Wang, Z. P. Zhao, M. N. Ding, X. Xu, C. Wang, S. J. Lee, Y. Huang, R. C. Chiechi, C. J. Lambert, X. F. Duan, *Sci. Adv.* **2018**, *4*, aat8237; c) T. Li, M. Jevric, J. R. Hauptmann, R. Hviid, Z. Wei, R. Wang, N. E. A. Reeler, E. Thyrhaug, S. Petersen, J. A. S. Meyer, N. Bovet, T. Vosch, J. Nygård, X. Qiu, W. Hu, Y. Liu, G. C. Solomon, H. G. Kjaergaard, T. Bjørnholm, M. B. Nielsen, B. W. Laursen, K. Nørgaard, *Adv. Mater.* **2013**, *25*, 4170.
[11] a) S. Seo, M. Min, J. Lee, T. Lee, S. Y. Choi, H. Lee, *Angew. Chem., Int. Ed.* **2011**, *51*, 112; b) A. V. Walker, T. B. Tighe, O. M. Cabarcos, M. D. Reinard, B. C. Haynie, S. Uppili, N. Winograd, D. L. Allara, *J. Am. Chem. Soc.* **2004**, *126*, 3954; c) G. L. Fisher, A. V. Walker, A. E. Hooper, T. B. Tighe, K. B. Bahnck, H. T. Skriba, M. D. Reinard, B. C. Haynie, R. L. Opila, N. Winograd, D. L. Allara, *J. Am. Chem. Soc.* **2002**, *124*, 5528.
[12] Y. C. Liu, R. L. McCreery, *J. Am. Chem. Soc.* **1995**, *117*, 11254.
[13] L. Yuan, N. Nerngchamnong, L. Cao, H. Hamoudi, E. del Barco, M. Roemer, R. K. Sriramula, D. Thompson, C. A. Nijhuis, *Nat. Commun.* **2015**, *6*, 6324.
[14] B. Long, M. Manning, M. Burke, B. N. Szafranek, G. Visimberga, D. Thompson, J. C. Greer, I. M. Povey, J. MacHale, G. Lejosne, D. Neumaier, A. J. Quinn, *Adv. Funct. Mater.* **2012**, *22*, 717.
[15] a) G. Wang, Y. Kim, M. Choe, T. W. Kim, T. Lee, *Adv. Mater.* **2011**, *23*, 760; b) V. B. Engelkes, J. M. Beebe, C. D. Frisbie, *J. Am. Chem. Soc.* **2004**, *126*, 14287; c) B. Xu, N. J. Tao, *Science* **2003**, *301*, 1221; d) H. Ju, J. Wang, W. Liu, J. Hao, M. Li, Y. Xu, B. Wang, S. He, K. Mei, C. H. Sue Andrew, K. Chen, C. Jia, X. Guo, *CCS Chem.* **2024**, https://doi.org/10.31635/ccschem.024.202403861.
[16] a) L. Jiang, C. S. S. Sangeeth, C. A. Nijhuis, *J. Am. Chem. Soc.* **2015**, *137*, 10659. b) T. Toledano, H. Sazan, S. Mukhopadhyay, H. Alon, K. Lerman, T. Bendikov, D. T. Major, C. N. Sukenik, A. Vilan, D. Cahen, *Langmuir* **2014**, *30*, 13596; c) M. Baghbanzadeh, F. C. Simeone, C. M. Bowers, K. C. Liao, M. Thuo, M. Baghbanzadeh, M. S. Miller, T. B. Carmichael, G. M. Whitesides, *J. Am. Chem. Soc.* **2014**, *136*, 16919.
[17] P. Song, D. Thompson, H. V. Annadata, S. Guerin, K. P. Loh, C. A. Nijhuis, *J. Phys. Chem. C* **2017**, *121*, 4172
[18] T. Li, J. R. Hauptmann, Z. Wei, S. Petersen, N. Bovet, T. Vosch, J. Nygård, W. Hu, Y. Liu, T. Bjørnholm, K. Nørgaard, B. W. Laursen, *Adv. Mater.* **2012**, *24*, 1333.

[19] J. Koo, Y. Jang, L. Martin, D. Kim, H. Jeong, K. Kang, W. Lee, J. Kim, W. T. Hwang, D. Xiang, E. Scheer, M. Kabdulov, T. Huhn, F. Pauly, T. Lee, *ACS Appl. Mater. Interfaces* **2019**, *11*, 11645.
[20] a) C. Jia, A. Migliore, N. Xin, S. Huang, J. Wang, Q. Yang, S. Wang, H. Chen, D. Wang, B. Feng, Z. Liu, G. Zhang, D. H. Qu, H. Tian, M. A. Ratner, H. Q. Xu, A. Nitzan, X. Guo, *Science* **2016**, *352*, 1443; b) P. Li, Y. Chen, B. Wang, M. Li, D. Xiang, C. Jia, X. Guo, *Opto-Electron. Adv.* **2022**, *5*, 210094.
[21] L. Zhou, M. Zhang, Y. Huo, L. Bai, S. He, J. Wang, C. Jia, X. Guo, *Green Energy Environ.* **2024**, https://doi.org/10.1016/j.gee.2024.01.003.
[22] a) C. Jia, W. Ma, J. Guan, C. Gu, X. Li, L. Meng, Y. Gong, S. Meng, X. Guo, *Adv. Electron. Mater.* **2017**, *3*, 1700211; b) C. Gu, C. Jia, X. Guo, *Mater. Chem. Front.* **2017**, *1*, 2125; c) C. Jia, W. Ma, C. Gu, H. Chen, H. Yu, X. Li, F. Zhang, L. Gu, A. Xia, X. Hou, S. Meng, X. Guo, *Nano. Lett.* **2016**, *16*, 3600.
[23] I. Chung, B. Lee, J. He, R. P. H. Chang, M. G. Kanatzidis, *Nature* **2012**, *485*, 486.
[24] C. Li, M. T. Cole, W. Lei, K. Qu, K. Ying, Y. Zhang, A. R. Robertson, J. H. Warner, S. Ding, X. Zhang, B. Wang, W. I. Milne, *Adv. Funct. Mater.* **2014**, *24*, 1218.
[25] J. Shin, S. Yang, J. S. Eo, T. Jeon, J. Lee, C. H. Lee, G. Wang, *Small Methods* **2022**, *6*, 2200646.
[26] a) Y. M. Seo, W. Jang, T. Gu, D. Whang, *Materials* **2020**, *13*, 2166; b) S. Dalgleish, L. Reissig, Y. Shuku, G. Ligorio, K. Awaga, E. J. W. List-Kratochvil, *Sci. Rep.* **2019**, *9*, 16682; c) J. Lu, A. Lipatov, N. S. Vorobeva, D. S. Muratov, A. Sinitskii, *Adv. Electron. Mater.* **2018**, *4*, 1800021; d) S. Presolski, M. Pumera, *Mater. Today* **2016**, *19*, 140; e) K. C. Knirsch, N. C. Berner, H. C. Nerl, C. S. Cucinotta, Z. Gholamvand, N. McEvoy, Z. Wang, I. Abramovic, P. Vecera, M. Halik, S. Sanvito, G. S. Duesberg, V. Nicolosi, F. Hauke, A. Hirsch, J. N. Coleman, C. Backes, *ACS Nano* **2015**, *9*, 6018.
[27] M. A. Stoeckel, M. Gobbi, T. Leydecker, Y. Wang, M. Eredia, S. Bonacchi, R. Verucchi, M. Timpel, M. V. Nardi, E. Orgiu, P. Samorì, *ACS Nano* **2019**, *13*, 11613.
[28] a) Y. D. Zhao, M. Gobbi, L. E. Hueso, P. Samori, *Chem. Rev.* **2022**, *122*, 50; b) S. Mouri, Y. Miyauchi, K. Matsuda, *Nano Lett.* **2013**, *13*, 5944;
[29] a) H. Sojoudi, J. Baltazar, L. M. Tolbert, C. L. Henderson, S. Graham, *ACS Appl. Mater. Interfaces* **2012**, *4*, 4781; b) Z. Yan, Z. Sun, W. Lu, J. Yao, Y. Zhu, J. M. Tour, *ACS Nano* **2011**, *5*, 1535.
[30] K. Yokota, K. Takai, T. Enoki, *Nano Lett.* **2011**, *11*, 3669.
[31] M. Gobbi, S. Bonacchi, J. X. Lian, Y. Liu, X. Y. Wang, M. A. Stoeckel, M. A. Squillaci, G. D'Avino, A. Narita, K. Müllen, X. Feng, Y. Olivier, D. Beljonne, P. Samorì, E. Orgiu, *Nat. Commun.* **2017**, *8*, 14767.
[32] a) A. Ziletti, A. Carvalho, D. K. Campbell, D. F. Coker, A. H. Castro Neto, *Phys. Rev. Lett.* **2015**, *114*, 046801; b) J. O. Island, G. A. Steele, H. S. J. v. d. Zant, A. Castellanos-Gomez, *2D Mater.* **2015**, *2*, 011002; c) J. D. Wood, S. A. Wells, D. Jariwala, K. S. Chen, E. Cho, V. K. Sangwan, X. Liu, L. J. Lauhon, T. J. Marks, M. C. Hersam, *Nano Lett.* **2014**, *14*, 6964.
[33] a) V. Artel, Q. Guo, H. Cohen, R. Gasper, A. Ramasubramaniam, F. Xia, D. Naveh, *NPJ 2D Mater. Appl.* **2017**, *1*, 6; b) C. R. Ryder, J. D. Wood, S. A. Wells, Y. Yang, D. Jariwala, T. J. Marks, G. C. Schatz, M. C. Hersam, *Nat. Chem.* **2016**, *8*, 597.
[34] a) Z. Yu, Y. Pan, Y. Shen, Z. Wang, Z. Y. Ong, T. Xu, R. Xin, L. Pan, B. Wang, L. Sun, J. Wang, G. Zhang, Y. W. Zhang, Y. Shi, X. Wang, *Nat. Commun.* **2014**, *5*, 5290; b) M. Amani, D. H. Lien, D. Kiriya, J. Xiao, A. Azcatl, J. Noh, S. R. Madhvapathy, R. Addou, S. Kc, M. Dubey, K. Cho, R. M. Wallace, S. C. Lee, J. H. He, J. W. Ager, X. Zhang, E. Yablonovitch, A. Javey, *Science* **2015**, *350*, 1065; c) S. Bertolazzi, S. Bonacchi, G. Nan, A. Pershin, D. Beljonne, P. Samorì, *Adv. Mater.* **2017**, *29*, 1606760.
[35] B. Lee, Y. Chen, F. Duerr, D. Mastrogiovanni, E. Garfunkel, E. Y. Andrei, V. Podzorov, *Nano Lett.* **2010**, *10*, 2427.
[36] C. Coletti, C. Riedl, D. S. Lee, B. Krauss, L. Patthey, K. von Klitzing, J. H. Smet, U. Starke, *Phys. Rev. B* **2010**, *81*, 235401.
[37] D. Liu, M. He, C. Huang, X. Sun, B. Gao, *J. Phys. Chem. C* **2017**, *121*, 10546.
[38] a) H. Liu, S. Ryu, Z. Chen, M. L. Steigerwald, C. Nuckolls, L. E. Brus, *J. Am. Chem. Soc.* **2009**, *131*, 17099; b) G. Gao, D. Liu, S. Tang, C. Huang, M. He, Y. Guo, X. Sun, B. Gao, *Sci. Rep.* **2016**, *6*, 20034.
[39] R. Nouchi, K.-i. Ikeda, *Phys. Chem. Chem. Phys.* **2020**, *22*, 1268.
[40] K. F. Mak, C. Lee, J. Hone, J. Shan, T. F. Heinz, *Phys. Rev. Lett.* **2010**, *105*, 136805.
[41] a) D. Kiriya, M. Tosun, P. Zhao, J. S. Kang, A. Javey, *J. Am. Chem. Soc.* **2014**, *136*, 7853; b) S. M. Kim, J. H. Jang, K. K. Kim, H. K. Park, J. J. Bae, W. J. Yu, I. H. Lee, G. Kim, D. D. Loc, U. J. Kim, E. H. Lee, H. J. Shin, J. Y. Choi, Y. H. Lee, *J. Am. Chem. Soc.* **2009**, *131*, 327; c) W. J. Yu, L. Liao, S. H. Chae, Y. H. Lee, X. Duan, *Nano Lett.* **2011**, *11*, 4759.
[42] Y. Li, C. Y. Xu, P. Hu, L. Zhen, *ACS Nano* **2013**, *7*, 7795.
[43] a) H. Fang, S. Chuang, T. C. Chang, K. Takei, T. Takahashi, A. Javey, *Nano Lett.* **2012**, *12*, 3788; b) W. Liu, J. Kang, D. Sarkar, Y. Khatami, D. Jena, K. Banerjee, *Nano Lett.* **2013**, *13*, 1983.
[44] a) S. Das, J. Appenzeller, *Appl. Phys. Lett.* **2013**, *103*, 103501; b) H. J. Chuang, X. Tan, N. J. Ghimire, M. M. Perera, B. Chamlagain, M. M.-C. Cheng, J. Yan, D. Mandrus, D. Tománek, Z. Zhou, *Nano Lett.* **2014**, *14*, 3594; c) J. K. Huang, J. Pu, C. L. Hsu, M. H. Chiu, Z. Y. Juang, Y. H. Chang, W. H. Chang, Y. Iwasa, T. Takenobu, L. J. Li, *ACS Nano* **2014**, *8*, 923; d) Y. J. Zhang, T. Oka, R. Suzuki, J. T. Ye, Y. Iwasa, *Science* **2014**, *344*, 725.
[45] H. G. Ji, P. Solís-Fernández, D. Yoshimura, M. Maruyama, T. Endo, Y. Miyata, S. Okada, H. Ago, *Adv. Mater.* **2019**, *31*, 1903613.
[46] A. Tarasov, S. Zhang, M. Y. Tsai, P. M. Campbell, S. Graham, S. Barlow, S. R. Marder, E. M. Vogel, *Adv. Mater.* **2015**, *27*, 1175.
[47] a) G. Vogt, G. Krampert, P. Niklaus, P. Nuernberger, G. Gerber, *Phys. Rev. Lett.* **2007**, *94*, 068305; b) X. Tong, M. Pelletier, A. Lasia, Y. Zhao, *Angew. Chem., Int. Ed.* **2008**, *47*, 3596.
[48] Y. Zhao, S. Bertolazzi, P. Samorì, *ACS Nano* **2019**, *13*, 4814.
[49] a) K. F. Mak, K. He, C. Lee, G. H. Lee, J. Hone, T. F. Heinz, J. Shan, *Nat. Mater.* **2013**, *12*, 207; b) J. S. Ross, S. Wu, H. Yu, N. J. Ghimire, A. M. Jones, G. Aivazian, J. Yan, D. G. Mandrus, D. Xiao, W. Yao, X. Xu, *Nat. Commun.* **2013**, *4*, 1474; c) K. He, N. Kumar, L. Zhao, Z. Wang, K. F. Mak, H. Zhao, J. Shan, *Phys. Rev. Lett.* **2014**, *113*, 026803.
[50] a) K. F. Mak, K. He, J. Shan, T. F. Heinz, *Nat. Nanotechnol.* **2012**, *7*, 494; b) H. Zeng, J. Dai, W. Yao, D. Xiao, X. Cui, *Nat. Nanotechnol.* **2012**, *7*, 490.
[51] J. Choi, H. Zhang, J. H. Choi, *ACS Nano* **2016**, *10*, 1671.
[52] D. H. Kang, M. S. Kim, J. Shim, J. Jeon, H. Y. Park, W. S. Jung, H. Y. Yu, C. H. Pang, S. Lee, J. H. Park, *Adv. Funct. Mater.* **2015**, *25*, 4219.
[53] N. Alidoust, G. Bian, S. Y. Xu, R. Sankar, M. Neupane, C. Liu, I. Belopolski, D. X. Qu, J. D. Denlinger, F. C. Chou, M. Z. Hasan, *Nat. Commun.* **2014**, *5*, 4673.
[54] J. D. Lin, C. Han, F. Wang, R. Wang, D. Xiang, S. Qin, X. A. Zhang, L. Wang, H. Zhang, A. T. S. Wee, W. Chen, *ACS Nano* **2014**, *8*, 5323.
[55] a) W. Choi, M. Y. Cho, A. Konar, J. H. Lee, G. B. Cha, S. C. Hong, S. Kim, J. Kim, D. Jena, J. Joo, S. Kim, *Adv. Mater.* **2012**, *24*, 5832; b) H. S. Lee, S. W. Min, Y. G. Chang, M. K. Park, T. Nam, H. Kim, J. H. Kim, S. Ryu, S. Im, *Nano Lett.* **2012**, *12*, 3695; c) O. Lopez-Sanchez, D. Lembke, M. Kayci, A. Radenovic, A. Kis, *Nat. Nanotechnol.* **2013**, *8*, 497; d) S. H. Yu, Y. Lee, S. K. Jang, J. Kang, J. Jeon, C. Lee, J. Y. Lee, H. Kim, E. Hwang, S. Lee, J. H. Cho, *ACS Nano* **2014**, *8*, 8285.
[56] a) R. F. Frindt, *Phys. Rev. Lett.* **1972**, *28*, 299; b) Z. Lin, A. McCreary, N. Briggs, S. Subramanian, K. Zhang, Y. Sun, X. Li, N. J. Borys, H. Yuan, S. K. Fullerton-Shirey, A. Chernikov, H. Zhao, S. McDonnell, A. M. Lindenberg, K. Xiao, B. J. LeRoy, M. Drndić, J. C. M. Hwang, J. Park, M. Chhowalla, R. E. Schaak, A. Javey, M. C. Hersam, J. Robinson, M. Terrones, *2D Mater.* **2016**, *3*, 042001; c) X. Xi, Z. Wang, W. Zhao, J.

H. Park, K. T. Law, H. Berger, L. Forró, J. Shan, K. F. Mak, *Nat. Phys.* **2016**, *12*, 139.
[57] a) S. Kezilebieke, M. Dvorak, T. Ojanen, P. Liljeroth, *Nano Lett.* **2018**, *18*, 2311; b) H. Alpern, K. Yavilberg, T. Dvir, N. Sukenik, M. Klang, S. Yochelis, H. Cohen, E. Grosfeld, H. Steinberg, Y. Paltiel, O. Millo, *Nano Lett.* **2019**, *19*, 5167; c) S. Kezilebieke, R. Žitko, M. Dvorak, T. Ojanen, P. Liljeroth, *Nano Lett.* **2019**, *19*, 4614.
[58] F. Calavalle, P. Dreher, A. P. Surdendran, W. Wan, M. Timpel, R. Verucchi, C. Rogero, T. Bauch, F. Lombardi, F. Casanova, M. V. Nardi, M. M. Ugeda, L. E. Hueso, M. Gobbi, *Nano Lett.* **2020**, *21*, 136.
[59] X. Xi, H. Berger, L. Forró, J. Shan, K. F. Mak, *Phys. Rev. Lett.* **2016**, *117*, 106801.
[60] S. Najmaei, X. Zou, D. Er, J. Li, Z. Jin, W. Gao, Q. Zhang, S. Park, L. Ge, S. Lei, J. Kono, V. B. Shenoy, B. I. Yakobson, A. George, P. M. Ajayan, J. Lou, *Nano Lett.* **2014**, *14*, 1354.
[61] Y. Zhao, S. Bertolazzi, M. S. Maglione, C. Rovira, M. Mas-Torrent, P. Samorì, *Adv. Mater.* **2020**, *32*, 2000740.
[62] K. Ueno, S. Nakamura, H. Shimotani, H. T. Yuan, N. Kimura, T. Nojima, H. Aoki, Y. Iwasa, M. Kawasaki, *Nat. Nanotechnol.* **2011**, *6*, 408.
[63] a) X. Chia, A. Ambrosi, D. Sedmidubský, Z. Sofer, M. Pumera, *Chem. - Eur. J.* **2014**, *20*, 17426; b) E. Marchante, N. Crivillers, M. Buhl, J. Veciana, M. Mas-Torrent, *Angew. Chem., Int. Ed.* **2016**, *55*, 368; c) Y. Wang, C. H. Kim, Y. Yoo, J. E. Johns, C. D. Frisbie, *Nano Lett.* **2017**, *17*, 7586.
[64] P. Fathi-Hafshejani, N. Azam, L. Wang, M. A. Kuroda, M. C. Hamilton, S. Hasim, M. Mahjouri-Samani, *ACS Nano* **2021**, *15*, 11461.
[65] a) E. J. H. Lee, K. Balasubramanian, R. T. Weitz, M. Burghard, K. Kern, *Nat. Nanotechnol.* **2008**, *3*, 486; b) D. W. Yue, C. H. Ra, X. C. Liu, D. Y. Lee, W. J. Yoo, *Nanoscale* **2014**, *7*, 825; c) A. Allain, J. Kang, K. Banerjee, A. Kis, *Nat. Mater.* **2015**, *14*, 1195; d) S. Wachter, D. K. Polyushkin, O. Bethge, T. Mueller, *Nat. Commun.* **2017**, *8*, 14948.
[66] a) B. Radisavljevic, A. Radenovic, J. Brivio, V. Giacometti, A. Kis, *Nat. Nanotechnol.* **2011**, *6*, 147. b) H. Kwon, W. Choi, D. Lee, Y. Lee, J. Kwon, B. Yoo, C. P. Grigoropoulos, S. Kim, *Nano Res.* **2014**, *7*, 1137.
[67] a) W. S. Leong, X. Luo, Y. Li, K. H. Khoo, S. Y. Quek, J. T. L. Thong, *ACS Nano* **2015**, *9*, 869; b) J. Wang, Q. Yao, C. W. Huang, X. Zou, L. Liao, S. Chen, Z. Fan, K. Zhang, W. Wu, X. Xiao, C. Jiang, W. W. Wu, *Adv. Mater.* **2016**, *28*, 8302; c) S. S. Chee, D. Seo, H. Kim, H. Jang, S. Lee, S. P. Moon, K. H. Lee, S. W. Kim, H. Choi, M. H. Ham, *Adv. Mater.* **2019**, *31*, 1804422.
[68] S. Das, H. Y. Chen, A. V. Penumatcha, J. Appenzeller, *Nano Lett.* **2013**, *13*, 100.
[69] K. Cho, J. Pak, J. K. Kim, K. Kang, T. Y. Kim, J. Shin, B. Y. Choi, S. Chung, T. Lee, *Adv. Mater.* **2018**, *30*, 1705540.
[70] a) M. Farmanbar, G. Brocks, *Phys. Rev. B* **2015**, *91*, 161304; b) M. Farmanbar, G. Brocks, *Adv. Electron. Mater.* **2016**, *2*, 1500405.
[71] A. Matković, A. Petritz, G. Schider, M. Krammer, M. Kratzer, E. Karner-Petritz, A. Fian, H. Gold, M. Gärtner, A. Terfort, C. Teichert, E. Zojer, K. Zojer, B. Stadlober, *Adv. Electron. Mater.* **2020**, *6*, 2000110.
[72] a) S. L. Li, K. Tsukagoshi, E. Orgiu, P. Samorì, *Chem. Soc. Rev.* **2016**, *45*, 118. b) A. Petritz, M. Krammer, E. Sauter, M. Gärtner, G. Nascimbeni, B. Schrode, A. Fian, H. Gold, A. Cojocaru, E. Karner-Petritz, R. Resel, A. Terfort, E. Zojer, M. Zharnikov, K. Zojer, B. Stadlober, *Adv. Funct. Mater.* **2018**, *28*, 1804462.
[73] Y. Cao, Z. Wei, S. Liu, L. Gan, X. Guo, W. Xu, M. L. Steigerwald, Z. Liu, D. Zhu, *Angew. Chem., Int. Ed.* **2010**, *49*, 6319.
[74] a) C.-A. Di, D. Wei, G. Yu, Y. Liu, Y. Guo, D. Zhu, *Adv. Mater.* **2008**, *20*, 3289; b) Y. Cao, S. Liu, Q. Shen, K. Yan, P. Li, J. Xu, D. Yu, M. L. Steigerwald, C. Nuckolls, Z. Liu, X. Guo, *Adv. Funct. Mater.* **2009**, *19*, 2743.
[75] M. El Abbassi, S. Sangtarash, X. Liu, M. L. Perrin, O. Braun, C. Lambert, H. S. J. van der Zant, S. Yitzchaik, S. Decurtins, S. X. Liu, H. Sadeghi, M. Calame, *Nat. Nanotechnol.* **2019**, *14*, 957.
[76] A. R. Beal, W. Y. Liang, *Philos. Mag. (Abingdon)* **1973**, *27*, 1397.
[77] a) O. Mashtalir, M. Naguib, V. N. Mochalin, Y. Dall'Agnese, M. Heon, M. W. Barsoum, Y. Gogotsi, *Nat. Commun.* **2013**, *4*, 1716; b) O. Mashtalir, M. R. Lukatskaya, M. Q. Zhao, M. W. Barsoum, Y. Gogotsi, *Adv. Mater.* **2015**, *27*, 3501.
[78] a) C. Wang, Q. He, U. Halim, Y. Liu, E. Zhu, Z. Lin, H. Xiao, X. Duan, Z. Feng, R. Cheng, N. O. Weiss, G. Ye, Y. C. Huang, H. Wu, H. C. Cheng, I. Shakir, L. Liao, X. Chen, W. A. Goddard Iii, Y. Huang, X. Duan, *Nature* **2018**, *555*, 231; b) W. He, H. Zang, S. Cai, Z. Mu, C. Liu, M. Ding, P. Wang, X. Wang, *Nano Res.* **2020**, *13*, 2917; c) S. Yang, P. Zhang, A. S. Nia, X. Feng, *Adv. Mater.* **2020**, *32*, 1907857.
[79] J. Sun, M. Sadd, P. Edenborg, H. Grönbeck, P. H. Thiesen, Z. Xia, V. Quintano, R. Qiu, A. Matic, V. Palermo, *Sci Adv.* **2021**, *7*, 0812.
[80] Q. Cao, F. Grote, M. Huβmann, S. Eigler, *Nanoscale Adv.* **2021**, *3*, 963.
[81] Q. He, Z. Lin, M. Ding, A. Yin, U. Halim, C. Wang, Y. Liu, H. C. Cheng, Y. Huang, X. Duan, *Nano Lett.* **2019**, *19*, 6819.
[82] N. Wang, H. Tang, M. Shi, H. Zhang, W. Zhuo, D. Liu, F. Meng, L. Ma, J. Ying, L. Zou, Z. Sun, X. Chen, *J. Am. Chem. Soc.* **2019**, *141*, 17166.
[83] a) A. A. Soluyanov, D. Gresch, Z. Wang, Q. Wu, M. Troyer, X. Dai, B. A. Bernevig, *Nature* **2015**, *527*, 495; b) K. Deng, G. Wan, P. Deng, K. Zhang, S. Ding, E. Wang, M. Yan, H. Huang, H. Zhang, Z. Xu, J. Denlinger, A. Fedorov, H. Yang, W. Duan, H. Yao, Y. Wu, S. Fan, H. Zhang, X. Chen, S. Zhou, *Nat. Phys.* **2016**, *12*, 1105.
[84] a) C. Pauly, B. Rasche, K. Koepernik, M. Liebmann, M. Pratzer, M. Richter, J. Kellner, M. Eschbach, B. Kaufmann, L. Plucinski, C. M. Schneider, M. Ruck, J. van den Brink, M. Morgenstern, *Nat. Phys.* **2015**, *11*, 338; b) R. Noguchi, T. Takahashi, K. Kuroda, M. Ochi, T. Shirasawa, M. Sakano, C. Bareille, M. Nakayama, M. D. Watson, K. Yaji, A. Harasawa, H. Iwasawa, P. Dudin, T. K. Kim, M. Hoesch, V. Kandyba, A. Giampietri, A. Barinov, S. Shin, R. Arita, T. Sasagawa, T. Kondo, *Nature* **2019**, *566*, 518; c) H. X. Zhang, A. Rousuli, S. C. Shen, K. N. Zhang, C. Wang, L. P. Luo, J. Z. Wang, Y. Wu, Y. Xu, W. H. Duan, H. Yao, P. Yu, S. Y. Zhou, *Sci. Bull.* **2020**, *65*, 188.
[85] C. Wan, X. Gu, F. Dang, T. Itoh, Y. Wang, H. Sasaki, M. Kondo, K. Koga, K. Yabuki, G. J. Snyder, R. Yang, K. Koumoto, *Nat. Mater.* **2015**, *14*, 622.
[86] G. H. Kim, L. Shao, K. Zhang, K. P. Pipe, *Nat. Mater.* **2013**, *12*, 719.

Mengmeng Li received her B.S. degree in 2021 from the College of Electronic Information Engineering, Hebei University of Technology. She is currently a Ph.D. candidate with Prof. Xuefeng Guo and Prof. Chuancheng Jia at the College of Electronic Information and Optical Engineering, Nankai University. Her current research is focused on vertical heterojunction devices.

Yu Jiang received his B.S. degree in 2021 from the College of Electrical and Information Engineering, Changchun Institute of Technology. He is currently a master student with Prof. Xuefeng Guo and Prof. Chuancheng Jia at College of Electronic Information and Optical Engineering, Nankai University. His current research is focused on single-molecule devices.

Hongyu Ju received his M.S. degree in 2020 from School of Life Science and Engineering, Southwest Jiaotong University. He is currently a Ph.D. candidate at School of Pharmaceutical Science and Technology, Tianjin University and Center of Single-Molecule Sciences, Nankai University, under the supervision of Prof. Kunrong Mei, Prof. Xuefeng Guo and Prof. Chuancheng Jia. His research focuses on single-molecule electronics and supramolecular chemistry.

Suhang He obtained her Ph.D. from Wuhan University in 2014. She then worked at Hisun Pharmaceuticals and the SGS Guangzhou branch from 2015 to 2018. Between 2019 and 2023, she was a postdoctoral researcher in the lab of Prof. Werner Nau at Constructor University. Currently, she is an associate professor at Nankai University, where her research focuses on supramolecular electronics and supramolecular chemistry.

Chuancheng Jia received his Ph.D. degree in 2014 from the College of Chemistry and Molecular Engineering, Peking University, under the guidance of Prof. Xuefeng Guo. From 2014 to 2020, he was a postdoc at Institute of Chemistry, Chinese Academy of Sciences and University of California, Los Angeles. He joined the faculty as a professor at Nankai University in 2020. His research is focused on single-molecule electronics and dynamics.

Xuefeng Guo received his B.S. degree in 1998 from Beijing Normal University and his Ph.D. degree in 2004 from Institute of Chemistry, Chinese Academy of Sciences, Beijing. From 2004 to 2007, he was a postdoc at the Columbia University Nanocenter. He joined the faculty as a professor under "Peking 100-Talent" Program at Peking University in 2008. His current research is focused on single-molecule science and technology.